Corticosterone inhibits GAS6 to govern hair follicle stem-cell quiescence

Sekyu Choi, Bing Zhang, Sai Ma, Meryem Gonzalez-Celeiro, Daniel Stein, Xin Jin, Seung Tea Kim, Yuan-Lin Kang, Antoine Besnard, Amelie Rezza, et al.

Published in final edited form as:

Nature. 2021 April ; 592(7854): 428–432. doi:10.1038/s41586-021-03417-2.

Corticosterone inhibits Gas6 to govern hair follicle stem cell quiescence

Sekyu Choi[1,2], **Bing Zhang**[1,2,14], **Sai Ma**[1,3,9], **Meryem Gonzalez-Celeiro**[1,2], **Daniel Stein**[1,2], **Xin Jin**[4], **Seung Tea Kim**[1,2], **Yuan-Lin Kang**[1,2], **Antoine Besnard**[2,5,6,15], **Amelie Rezza**[7,8,16], **Laura Grisanti**[7,8], **Jason Buenrostro**[1,2,9], **Michael Rendl**[7,8,10], **Matthias Nahrendorf**[11,12,13], **Amar Sahay**[2,5,6,9], **Ya-Chieh Hsu**[1,2,*]

[1]Department of Stem Cell and Regenerative Biology, Harvard University, Cambridge, MA, USA.

[2]Harvard Stem Cell Institute, Cambridge, MA, USA.

[3]Department of Biology and Koch Institute, MIT, Cambridge, MA, USA.

[4]Society of Fellows, Harvard University, Cambridge MA, USA.

[5]Center for Regenerative Medicine, Massachusetts General Hospital, Boston, MA, USA.

[6]Department of Psychiatry, Massachusetts General Hospital, Harvard Medical School, Boston, MA, USA.

[7]Black Family Stem Cell Institute, Icahn School of Medicine at Mount Sinai, New York, NY, USA.

[8]Department of Cell, Developmental and Regenerative Biology, Icahn School of Medicine at Mount Sinai, New York, NY, USA.

[9]Broad Institute of Harvard and MIT, Cambridge, MA, USA.

[10]Department of Dermatology, Icahn School of Medicine at Mount Sinai, New York, NY, USA.

[11]Center for Systems Biology and Department of Radiology, Massachusetts General Hospital Research Institute, Harvard Medical School, Boston, MA, USA.

[12]Cardiovascular Research Center, Massachusetts General Hospital, Harvard Medical School, Boston, MA, USA.

[13]Department of Internal Medicine I, University Hospital Wuerzburg, Wuerzburg, Germany.

[14]Present address: School of Life Science, Westlake University, Hangzhou, Zhejiang, China.

[*]Correspondence to: Correspondence and requests for materials should be addressed to Y-C.H. Ya-Chieh Hsu, PhD (**Lead Contact**), yachieh_hsu@harvard.edu.

AUTHOR CONTRIBUTIONS

Y-C.H. and S.C. conceived the project. S.C. performed most of the experiments. B.Z. and S.M. performed bioinformatic analysis. M.G-C., D.S., and S.T.K. performed experiments related to chronic unpredictable stress, corticosterone feeding, and adrenalectomy. X.J. and Y-L.K. generated RNA-seq libraries. A.R. and L.G. performed *GR* qRT-PCR for DP and DF samples. B.Z., J.D.B., M.R., M.N., A.S., and A.B. provided intellectual input. Y-C.H. and S.C. wrote the manuscript, with discussion and feedback from all co-authors.

COMPETING INTERESTS

A patent application is pending for this work (applicants: President and Fellows of Harvard College; inventors: Y.-C.H. and S.C.; aspect covered: methods and compositions for controlling hair growth). All of the other authors declare no competing interests.

ADDITIONAL INFORMATION

Supplementary information is available for this paper.

[15]Present address: CNRS, Institut de Génomique Fonctionnelle, Montpellier, F-34094, France.

[16]Present address: 4 genOway, Lyon, 69007, France.

Abstract

Chronic, sustained exposure to stressors can profoundly impact tissue homeostasis, although the mechanisms by which these changes occur are largely unknown. Here, we report the adrenal gland-derived stress hormone corticosterone (the rodent equivalent of cortisol) regulates hair follicle stem cell (HFSC) quiescence and hair growth in mice. Without systemic corticosterone, HFSCs enter substantially more rounds of the regeneration cycle throughout life. Conversely, under chronic stress, elevated corticosterone levels prolong HFSC quiescence and keep hair follicles in an extended resting phase. Mechanistically, corticosterone acts on dermal papilla (DP) to suppress the expression of a secreted factor, Growth Arrest Specific 6 (*Gas6*). Restoring *Gas6* expression overcomes stress-induced inhibition of HFSC activation and hair growth. Our work identifies corticosterone as a systemic inhibitor of HFSC activity via its impact on the niche, and demonstrates that removal of such inhibition drives HFSCs into frequent regeneration cycles with no observable defects long-term.

INTRODUCTION

Stem cells are regulated by intrinsic regulators as well as extrinsic signals from the niche[1–4]. However, how systemic factors regulate stem cell behaviours to couple tissue regeneration with diverse bodily changes remains poorly understood. To understand the mechanisms connecting systemic changes and stem cell behaviour, we explored the impact of chronic stress on HFSCs. The hair follicle cycles between rest (telogen) and growth (anagen)[5]. HFSCs are located at the bulge and hair germ and are quiescent except during early anagen, when they proliferate transiently to initiate tissue regeneration[6,7]. Chronic stress, which triggers elevation of corticosterone secreted from the adrenal glands, has been anecdotally associated with hair loss in humans[8]. Early work in mice showed topical application of betamethasone, a steroid that inhibits Glucocorticoid Receptor (GR), the receptor for corticosterone, inhibits anagen entry[9] and overexpression of GR embryonically leads to underdeveloped hair follicles[10]. By contrast, adrenalectomy, which removes the source of corticosterone, accelerates hair growth in rats, rabbits, and minks[11–13]. Despite these observations, the cellular and molecular mechanisms by which corticosterone regulates tissue regeneration remain largely unexplored.

RESULTS

Adrenalectomy activates HFSCs

To determine how hormones from the adrenal glands impact hair cycle, we surgically removed both adrenal glands on postnatal day 35 (P35), a time before mice enter their extended second telogen (Extended Data Fig. 1a). In sham-operated wild-type (C57BL/6) mice, the second telogen began around P43-P45 and lasted on average 58 ± 2 days. By contrast, adrenalectomized (ADX) mice (both male and female) had a significantly shorter telogen (~11 days) with precocious activation starting from the hair germ (Fig. 1a, b,

Extended Data Fig. 1a, b). Normally, HFSCs only proliferate in early anagen and quickly resume quiescence by mid-anagen[7]. In ADX mice, however, HFSCs, located in the bulge and the upper outer root sheath[14,15] (ORS), remained proliferative in late anagen (Fig. 1c, Extended Data Fig. 1c). At late anagen, hair follicles in the ADX mice were longer than those at the same anagen stage in sham controls (Extended Data Fig. 1d). Although the hair shaft in ADX mice also becomes longer, likely due to the enhanced HFSC proliferation, ADX mice did not display gross abnormalities in their skin and showed similar expression of HFSC markers (Extended Data Fig. 1e–i). For both sham and ADX mice, the bulge and upper ORS resumed quiescence in catagen, and anagen and catagen durations were similar between the two (Fig. 1c, d). These data suggest HFSCs in ADX mice spend less time in quiescence.

ADX mice enter anagen continuously

Monitoring hair cycle of sham and ADX mice for an extended time period revealed that in sham animals, telogen became progressively longer (2^{nd} telogen ~ 58±2 days, 3^{rd} telogen ~ 75±2 days, 4^{th} telogen ~ 95±4 days), and anagen entry became sporadic and asynchronized (Fig. 1d, e, Extended Data Fig. 1j, k). By contrast, hair follicles in ADX mice only stayed in telogen for about 2 weeks, and they repeatedly entered anagen in a synchronized fashion (Extended Data Fig. 1j). Over a ~16-month period following adrenalectomy, ADX mice went through ~10 synchronized hair cycles in their back skin, whereas sham mice entered anagen asynchronously and rarely, and only completed ~3 hair cycles within 16 months (Fig. 1e). Telogen became ~30 days long in 17–18 months old ADX mice, which is still significantly shorter than the length of 2^{nd} telogen in young sham animals and in sharp contrast to sham old animals at the same age (Extended Data Fig. 1k)[16,17]. ADX mice displayed a hair coat density similar to young mice and robust anagen entry at 18–22 months of age (Fig. 1f, Extended Data Fig. 1j, l, 2a). Aged ADX mice showed normal hair follicle morphology, the presence of different hair types, and an absence of aberrant overgrowth (Extended Data Fig. 2a–c). Moreover, HFSC numbers were maintained despite repeated anagen entry (Extended Data Fig. 2c). These data suggest that systemic factors secreted from the adrenal glands are key regulators of HFSC quiescence and indicate the ability of HFSCs to regenerate hair follicles in ADX mice does not decline after rounds of anagen entry.

Corticosterone regulates HFSC quiescence

The adrenal gland produces several hormones, including corticosterone, epinephrine, norepinephrine, and aldosterone[18] (Extended Data Fig. 2d). We quantified levels of each hormone and found that levels of corticosterone dropped most substantially and became barely detectable in ADX animals (Extended Data Fig. 2d, e). Supplementation with corticosterone effectively suppressed the aberrant activation of HFSCs in ADX mice (Fig. 2a, b, Extended Data Fig. 2f). Together, these results suggest that corticosterone secreted from the adrenal glands acts as a key systemic regulator to suppress anagen entry under normal physiological conditions.

Elevated corticosterone inhibits anagen

To test if elevated corticosterone levels inhibit HFSC activation, wild-type 2nd telogen mice were given supplemental corticosterone in drinking water[19], leading to enhanced circulating corticosterone levels (Fig. 2c, Extended Data Fig. 2g). Transient elevation of corticosterone had minimal impact on hair cycle (Extended Data Fig. 2h), but long-term supplementation prolonged telogen (Fig. 2c, Extended Data Fig. 2i). Corticosterone-fed mice did not display obvious changes in weight, skin thickness, or apoptosis (Extended Data Fig. 2j–l). Once corticosterone was removed, mice could enter anagen (Extended Data Fig. 2m), suggesting that the impact of corticosterone on HFSCs is reversible.

To examine changes in HFSCs under physiological contexts in which corticosterone levels are altered, we adapted a chronic unpredictable stress model (see methods)[20,21]. Stressed mice displayed elevated corticosterone levels and significantly extended telogen (Fig. 2d, Extended Data Fig. 3a–c). Consistent with this, adrenalectomy prevented prolonged telogen (Extended Data Fig. 3d). As aged mice, similar to stressed mice, display significantly extended telogen length (Extended Data Fig. 1j, k)[16,17], we asked if corticosterone is also responsible for the long telogen seen in aged mice. Indeed, older mice have elevated levels of corticosterone, and adrenalectomy in 17–18 month old mice also led to rapid anagen entry (Extended Data Fig. 3e, f). Collectively, our data show that elevated corticosterone levels, whether physiological (e.g., arising from chronic stress or aging) or exogenously provided, extend telogen length.

Corticosterone acts on Dermal Papilla

To identify cell types corticosterone acts on to regulate HFSC quiescence, we first depleted GR (the receptor for corticosterone) from HFSCs using K15-CrePGR, a driver expressed in HFSCs. Despite efficient depletion of *GR* in HFSCs, the *K15-CrePGR; GRfl/fl* mice did not display significant differences in telogen length (Extended Data Fig. 4a, b), indicating that corticosterone does not act on HFSCs directly.

We then asked if corticosterone acts on cells in the niche to influence stem cell activity. Dermal fibroblasts are a heterogenous population surrounding HFSCs. Some fibroblast subpopulations, including DP and adipocyte precursor cells, can regulate HFSC activity[22,23]. To test if corticosterone regulates HFSC activity via fibroblasts, we depleted GR using Pdgfra-CreER, a driver expressed in the majority of fibroblast populations including DP and adipocyte precursor cells[24] (Fig. 3a, Extended Data Fig. 4c). Similar to ADX animals, *Pdgfra-CreER; GRfl/fl* mice displayed precocious anagen entry, and their bulge and upper ORS continued to proliferate in full anagen (Fig. 3b, Extended Data Fig. 4d, e). *Pdgfra-CreER; GRfl/fl* mice, like ADX mice, also continued to enter anagen with short telogen in between (Extended Data Fig. 4f–h).

qRT-PCR data show that DP expresses a higher level of GR than the rest of the fibroblasts (Extended Data Fig. 5a). To determine if DP mediates the effect of corticosterone, we deleted GR using Sox2-CreER, a driver expressed in a subset of DP[25,26]. Analysis of *Sox2-CreER; Rosa-YFP* mice suggested that CreER is active in the DP of guard hairs and absent in other hair follicle types (Fig. 3c, Extended Data Fig. 5b). Similarly, *Sox2-CreER; GRfl/fl*

animals had GR depletion only in the guard hair DP (2–3% of total hair follicles) (Extended Data Fig. 5c). These animals displayed precocious anagen entry and entered more rounds of hair cycle only in guard hair follicles, but not in other hair follicles where Sox2-CreER activity was absent (Fig. 3d, e, Extended Data Fig. 5d). Full anagen *Sox2-CreER; GRfl/fl* guard hair follicles were also more proliferative in their bulge and upper ORS region and grew longer hair shafts (Extended Data Fig. 5e–g). Together, these results indicate that DP plays a key role in mediating corticosterone's effect on prolonging telogen.

Corticosterone alters HFSC transcriptome

To explore molecular changes in HFSCs influenced by corticosterone, we performed RNA-sequencing (RNAseq) on FACS-purified HFSCs from sham, ADX, ADX+corticosterone, *Pdgfra-CreER* control, and *Pdgfra-CreER; GR fl/fl* animals (all in telogen). We first did pairwise comparisons between samples (sham vs. ADX; ADX vs. ADX+corticosterone; control vs. *Pdgfra-CreER; GRfl/fl*) to identify differentially expressed genes (1.5-fold change, $P_{adj} < 0.05$) and looked for overlap between these datasets (Fig. 3f, Extended Data Fig. 6a, b). This revealed 121 common differentially expressed genes, 54 of which are related to cell cycle regulation or cytokinesis machineries (Fig. 3g, Extended Data Fig. 6c). By contrast, signalling pathways and transcription factors known to regulate HFSC quiescence[2–4,7,27–30] were not significantly altered (Extended Data Fig. 6d). RNAseq showed that HFSCs in ADX have up-regulated cell cycle/division machineries despite being phenotypically quiescent, suggesting they are primed for activation. Moreover, these cell cycle-related genes were down-regulated to levels similar to sham controls when the ADX mice were fed with corticosterone, indicating that these molecular changes are downstream of corticosterone (Extended Data Fig. 6c). Given that these genes also overlapped with those differentially expressed in HFSCs purified from *Pdgfra-CreER; GRfl/fl mice*, our RNAseq data further support the idea that dermal fibroblasts relay the effect of corticosterone to HFSCs (Extended Data Fig. 6c).

To validate these molecular changes, we selected 7 core genes (*Aurkb*, *Ccnb1*, *Ccnb2*, *Cdca2*, *Rad51*, *Prc1*, and *Cdk1*) representing different cell cycle or cytokinesis-related categories to verify with qRT-PCR, and all were confirmed using independent biological sample sets (Extended Data Fig. 6d–f). Moreover, these 7 genes became down-regulated in HFSCs isolated from mice subjected to chronic unpredictable stress as well as mice fed with corticosterone, but displayed no changes in the epidermis, further underscoring that they represent the molecular changes in HFSCs downstream of systemic corticosterone (Extended Data Fig. 7a–d).

Gas6 is up-regulated in the DP upon ADX

Next, we aimed to identify dermal genes that relay the effect of corticosterone to HFSCs. For this, we conducted RNAseq using FACS-enriched DP cells from sham and ADX animals. In parallel, we also conducted RNAseq of DP from control and *Pdgfra-CreER; GRfl/fl* animals (Extended Data Fig. 7e). To avoid changes simply tracked with different hair cycle stages, all samples were taken at telogen (Extended Data Fig. 7f–h). From these, we identified differentially expressed genes (1.5-fold change, $P_{adj} < 0.05$) in DP upon adrenalectomy or dermal GR depletion (Extended Data Fig. 7i, j). As DP likely exert

regulatory effects on HFSCs via secreted proteins, we also conducted comparative secretome analyses to identify differentially expressed secreted factors in ADX or dermal GR-knockout DP cells (see methods). This approach identified a total of 7 shared secreted factors whose expression levels were significantly altered in the DP of both ADX animals and *Pdgfra-CreER; GRfl/fl* animals (Extended Data Fig. 8a). Among the candidate secreted factors, *Gas6* stood out as being abundantly expressed and significantly up-regulated (Extended Data Fig. 8b, c). *Gas6* encodes a gamma-carboxyglutamic acid-containing secreted protein and predominantly binds to AXL, a member of the TYRO3, AXL, and MERTK (TAM) family of receptor tyrosine kinases[31]. We confirmed by *in situ* hybridization that *Gas6* is up-regulated in the DP of ADX animals and returns to baseline levels when ADX animals are fed with corticosterone (Fig. 4a). In full anagen, *Gas6* levels are down-regulated in control DP but remain high in the ADX DP. *Gas6* signals are down-regulated in catagen in both control and ADX animals (Extended Data Fig. 8d). Moreover, HFSCs at both bulge and hair germ express its receptor *Axl*, whereas the matrix and epidermis have significantly lower levels of *Axl* (Extended Data Fig. 8e, f). Of all three TAM receptors, *Axl* is most highly expressed in HFSCs (Extended Data Fig. 8g).

GAS6 relays the effect of corticosterone

To examine the function of GAS6 in HFSC regulation, we FACS-purified HFSCs, plated them in culture, and added recombinant GAS6 protein to the media. HFSCs formed more colonies in the presence of GAS6 (Fig. 4b). Moreover, blocking AXL activity with the AXL-specific inhibitor R428 inhibited Gas6's ability to promote HFSC proliferation *in vitro* (Extended Data Fig. 8h). To evaluate the potency of GAS6 in promoting HFSC activation *in vivo*, we generated and packaged CAG-GFP and CAG-Gas6 into adeno-associated viruses (AAVs) and injected these AAVs into the skin through intradermal injections (Fig. 4c, Extended Data Fig. 9a). qRT-PCR confirmed that *Gas6* transcripts were up-regulated in the dermal fibroblasts in the AAV injected regions (Extended Data Fig. 9b). AAV-CAG-Gas6 injection promoted precocious anagen entry at the site of injection (Fig. 4c). Similar to ADX and *Pdgfra-CreER GRfl/fl* animals, HFSCs continued to proliferate at full anagen when *Gas6* was overexpressed, but cells in no other compartment did (Extended Data Fig. 9c–g). In addition, the 7 shared core genes up-regulated in ADX mice also became up-regulated in HFSCs upon *Gas6* overexpression (Extended Data Fig. 9h). Among the 7 shared core genes, *Cdk1, Ccnb1,* and *Rad51* have been reported as downstream targets of the GAS6-AXL pathway[32–34], supporting the idea that GAS6 is relaying corticosterone's effect to HFSCs.

We next tested the effect of the AXL inhibitor R428 *in vivo*. Topical application of R428 to ADX mice suppressed precocious anagen entry, suggesting that blocking the GAS6-AXL pathway can in part suppress the aberrant HFSC activity seen with loss of corticosterone (Extended Data Fig. 9i). Molecularly, R428 also suppressed the expression of the 7 core-signature genes upregulated in HFSCs isolated from ADX mice (Extended Data Fig. 9j). Together, these data confirm the role of the corticosterone-GAS6-AXL axis in regulating HFSC activity.

BMPs also suppress Gas6

Interestingly, *Gas6* expression in DP is low in early (refractory) telogen and up-regulated in late (competent) telogen (Extended data Fig. 10a), in agreement with previously reported DP microarray data[6]. Since corticosterone levels are relatively constant at different telogen stages (Extended Data Fig. 3e), we reasoned additional upstream signals, such as BMPs, might also regulate *Gas6* levels. BMPs are secreted from fibroblasts and dermal adipocytes to promote HFSC quiescence and have high levels in early telogen but low levels in late telogen[4,6]— the opposite trend we observed for *Gas6*. To test if BMPs regulate Gas6, we used AAV to overexpress NOGGIN, a secreted BMP inhibitor, and we saw elevated *Gas6* levels, suggesting that BMP suppresses *Gas6* expression (Extended Data Fig. 10a, b). Moreover, suppressing BMP signalling with NOGGIN in ADX mice led to significantly higher *Gas6* expression than in ADX or NOGGIN overexpression alone and further reduced telogen length relative to ADX mice (Extended Data Fig.10a–c). These data suggest that corticosterone (a systemic hormone) and BMP (a niche signal) represent two upstream signals that both suppress *Gas6* levels in DP.

Restoring Gas6 overcomes stress effects

Lastly, we asked whether the mechanisms identified here might be harnessed to counteract the effects of elevated corticosterone and promote HFSC activation under stress. To this end, we first tested if extended telogen is shortened by depleting GR specifically in dermal fibroblasts in chronically stressed mice (Extended Data Fig. 10d). Indeed, *Pdgfra-CreER; GRfl/fl* mice displayed significantly shorter telogen compared to control mice under chronic stress (Extended Data Fig. 10d). We then assessed *Gas6* levels in DP isolated from stressed mice and mice fed with corticosterone, finding that *Gas6* were significantly down-regulated in DP upon stress or elevation of corticosterone (Extended Data Fig. 10e, f).

To determine if restoring *Gas6* expression is sufficient to overcome stress-induced inhibition on HFSCs, we injected AAV-CAG-Gas6 intradermally and subjected the mice to chronic unpredictable stress or long-term corticosterone feeding (Fig. 4d). Overexpression of *Gas6* effectively mitigated prolonged telogen caused by either condition (Fig. 4d), suggesting that restoration of *Gas6* expression is sufficient to promote HFSC activation in a high corticosterone environment. Together, our data suggest that corticosterone regulates HFSC activity by inhibiting *Gas6* in the DP (Fig. 4e).

Discussion

Stem cells integrate both local and systemic inputs to couple tissue regeneration with the animal's overall physiological state (Supplementary Discussion). Here, we unravel a mechanism by which a systemic factor regulates a stem cell population by inhibiting a niche factor. Previous findings have suggested several mechanisms by which acute stress affects melanocyte stem cells or hair follicle biology[35–37]. Our results now suggest chronic stress delays anagen entry via a distinct mechanism. Our findings not only reveal important regulators of HFSC quiescence and activation at both local and systemic levels, but also identify the cellular and molecular mechanisms by which chronic stress influences the hair cycle (Extended Data Fig. 10g). Moreover, we demonstrate that the tissue regeneration

capacity of HFSCs remains robust even upon significantly increased rounds of anagen entry throughout life (Supplementary Discussion). Therefore, it may be possible to exploit HFSCs' ability to promote hair follicle regeneration by modulating the corticosterone-Gas6 axis.

METHODS

Randomization

Mice were randomly assigned to control or experimental groups whenever possible, except in experiments that required specific genotypes (littermate controls were used in these experiments).

Blinding

For LC-MS/MS analysis, RNA-seq library preparation, and sequencing, experimenters were blinded to experimental conditions. Blinding was not possible in mouse studies when specific genotypes or surgical models had to be identified according to experimental designs.

Animals

C57BL/6J, *GR fl/fl*[38], *K15-CrePGR*[39], *Pdgfra-CreER*[40], *Sox2-CreER*[41], and *R26-lsl-YFP*[42] mice were obtained from the Jackson Laboratory. Given the inherent differences in the timing of the hair cycle in wild-type male and female mice and that male mice start to fight >P70, confounding hair cycle analyses, we presented data from female mice for most experiments. However, consistent trends were observed in both males and females. For ADX and CORT-fed mice, we included results from both male and female mice, and the data are presented separately (female data: Fig. 1a, 2c; male data: Extended Data Fig. 1b, 2i). For GR knockout experiments, sex-matched littermates without Cre or without GR *fl/fl* were used as controls. All the control animals received the same dosage of tamoxifen (in the case of Pdgfra-CreER and Sox2-CreER) or RU486 (in the case of K15-CrePGR) as the experimental animals. The mice were maintained in an Association for Assessment and Accreditation of Laboratory Animal Care-approved animal facility. All procedures were approved by the Institutional Animal Care and Use Committee at Harvard University or the Icahn School of Medicine at Mount Sinai. Mice were housed in individually ventilated cages at a maximum density of 5 mice per cage with nestlet bedding and a red hut for enrichment and kept on a 12-h light–dark cycle. Room temperature was maintained at 22°C ± 1°C with 30%–70% humidity. Mice were fed ad libitum with rodent diet (Prolab IsoPro RMH 3000 5P75) and water. None of the mice were involved in any previous procedures prior to the study.

Adrenalectomy

C57BL/6J mice were anesthetized and small incisions were made on the back skin directly above each adrenal gland. Both adrenal glands were removed with a pair of curved forceps. Sham-operated mice (sham) underwent the same procedures as the ADX mice, except their adrenal glands were not removed. Because adrenal glands also secrete aldosterone to regulate salt balance, drinking water was supplemented with 1% w/v saline solution for both ADX and sham mice.

Chemical treatment and viral injection

4% RU486 (TCI America, Cat #M1732) in ethanol was used to induce *K15-CrePGR.* RU486 was applied topically once per day for 10 days to *K15-CrePGR; GR fl/fl* and sex-matched, littermate controls. Tamoxifen (Millipore Sigma, T5648) was dissolved in corn oil to a final concentration of 20 mg/ml and was used to induce *CreER* recombinase. Tamoxifen was injected into *Pdgfra-CreER; GR fl/fl*, *Sox2-CreER GR fl/fl*, and sex-matched, littermate controls intraperitoneally once per day for 4 to 6 days. To inhibit AXL activity, R428[ref43] (APExBIO, A8329; 2 mM in ethanol) was applied to ADX mice topically once a day. EdU (Lumiprobe Corporation, Cat #10540; 25 mg/kg) was administered by intraperitoneal injections. AAVs were produced as described previously[1,44] and injected directly into the dermis through intradermal injections. 2-month-old C57BL/6J mice were injected with AAV-GFP, AAV-Gas6, or AAV-Noggin (5×10^{10} genome copy number per animal).

Hair cycle analysis

Hair cycle progression was documented by standardized photographs at the start of each experiment and weekly thereafter. Anagen was determined by darkening of the skin followed by hair growth as previously described[5,45]. The back skin of mice was shaved with an electric clipper to reveal skin colour changes and hair coat recovery. Once the hair coat recovery reached ~90% of the back skin, the mice were shaved again to monitor the entry into next anagen. To assess the length of each hair cycle phase (telogen, anagen, catagen) of sham and ADX mice (P43-P140), skin colour changes were documented every 2–3 days. The length of each hair cycle was quantified as described previously[4] and was confirmed by histological section analysis.

Analysis of hair shaft length and type

Mice were shaved before ADX surgery or tamoxifen treatment to trim off the original hair coat. The mice were then followed through a complete anagen cycle and hair shafts (actual hairs) were plucked in the following telogen after anagen was completed. Individual hair shafts were sorted according to hair type (based on their unique banding patterns), and the shaft lengths were measured and analysed under a Keyence BX-700 microscope with x4, x20 or x40 objectives.

Chronic corticosterone feeding

35 μg/ml corticosterone (Millipore Sigma, C2505) was dissolved in 0.45% hydroxypropyl-β-cyclodextrin and added to the drinking water during the entire corticosterone feeding period[19]. Corticosterone water was changed every 3 days to prevent degradation. Control animals received vehicle water (0.45% hydroxypropyl-β-cyclodextrin).

Chronic unpredictable stress

Chronic unpredictable stress was adapted from protocols described previously[20,21]. C57BL/6 mice, sham, ADX, *Pdgfra-CreER GR fl/fl* mice, and their littermate controls were exposed to diverse stressors for 9 weeks. Two of the following stressors were applied each day in a randomized fashion: cage tilt, isolation, crowding, damp bedding, rapid light–dark

changes, restraining, empty cage, and 3x cage changes. See also Supplementary Discussion for a discussion of different stress models.

ELISA

Blood corticosterone levels were measured by ELISA (ARBOR assays, K014-H1) according to the manufacturer's instructions. Serum was collected by the tail clip bleeding method into heparinized tubes (Microvette® CB 300 LH (16.443.100) or Microvette® 300 LH (20.1309.100), Sarstedt Inc.) between 10 a.m. and 12 p.m.

Liquid chromatography-tandem mass spectrometry

Blood epinephrine and norepinephrine were measured by liquid chromatography-tandem mass spectrometry (LC-MS/MS). A stable isotope-labelled internal standard (d6-epinephrine, Cambridge Isotope Laboratories Inc., E-077) was used for absolute quantification. The standards for the HPLC system were prepared using a catecholamine mixture (epinephrine and norepinephrine) (Millipore Sigma, C-109). All samples were analysed on an Agilent 6460 Triple Quadrupole with an Agilent 1290 Infinity LC system.

Histology and immunohistochemistry

Skin samples were fixed in 4% paraformaldehyde (PFA, Electron Microscopy Sciences, Cat #15713) for 15 min at room temperature, washed in phosphate buffered saline (PBS), immersed in 30% sucrose solution overnight at 4°C, and embedded in optimal cutting temperature compound (O.C.T., Sakura Finetek, Cat #4583). Sections of approximately 35–50 μm were fixed in 4% PFA for 2 min and washed with PBS and 0.1% Triton X-100 in PBS. The slides were then blocked in blocking buffer (5% Donkey serum, 1% bovine serum albumin, 2% cold-water fish gelatin in 0.3% Triton X-100 in PBS) for 1 h at room temperature, incubated with primary antibodies overnight at 4°C, and incubated with secondary antibodies for 2–4 h at room temperature. The following antibodies and dilutions were used: CD34 (eBioscience, 14–0341-82, 1:100), CD140a (R&D Systems, AF1062, 1:100), P-Cadherin (R&D Systems, AF761, 1:400), GFP (Abcam, ab290, 1:5000), Cleaved Caspase-3 (Cell Signaling Technology, 9661S, 1:300), Sox9 (Millipore Sigma, AB5535, 1:500), phosphorylated histone H3 (Cell Signaling Technology, 3377S, 1:500) and Glucocorticoid Receptor (Cell Signaling Technology, 3660S, 1:100). DAPI was used as a counterstain for the nucleus. Cell proliferation assays were performed using a Click-It EdU Proliferation kit (Thermo Fisher Scientific, C10337) according to the manufacturer's instructions. Hematoxylin and eosin (H&E) staining was performed according to standard protocols.

In situ hybridization

Unfixed dorsal skin samples were collected and embedded in O.C.T. *In* situ hybridization was performed using the RNAscope® 2.5 HD detection kit (Red) (322360, Advanced Cell Diagnostics) with *Gas6* probe (450941, Advanced Cell Diagnostics), *Axl* probe (450931, Advanced Cell Diagnostics), or negative control probe (bacterial gene *DapB*, 310043, Advanced Cell Diagnostics) according to the manufacturer's protocol. Mean pixel intensities were measured using ImageJ (v1.52h).

Fluorescence-activated cell sorting (FACS)

Dermal cells were isolated as described[6,24,44,46,47]. Mouse dorsal skin was dissected and treated with collagenase in Hank's Balanced Salt Solution for 20–30 min at 37°C on an orbital shaker. The dermal fraction was collected by scraping followed by centrifugation at 300 g for 10 min. Dermal single-cell suspensions were obtained after 0.25% trypsin treatment for 10–20 min at 37°C followed by filtering and centrifugation. Samples were stained for 30 min on ice. The following antibodies were used: Pdgfra-biotin (eBioscience, 13–1401-82,1:250), CD45-eflour450 (eBioscience, 48–0451-82; 1:250), CD31-PE-Cy7 (eBioscience, 25–0311-81, 1:200), Sca-1-PerCP-Cy5.5 (eBioscience, 45–5981-82, 1:1000), CD24-FITC (eBioscience, 11–0242-82; 1:250), and Streptavidin-APC (eBioscience, 17–4317-82, 1:500). DAPI was used to exclude dead cells. DP cells were enriched as $CD45^{-}$, $CD31^{-}$, $Pdgfra^{+}$, $CD24^{-}$, $Sca\text{-}1^{-}$ cells , as described and validated previously[24,44]. The FACS strategy was further validated by the enrichment of DP signature genes[46–48] (Extended Data Fig. 7h).

For the isolation of HFSCs, mouse dorsal skin was dissected and the fat layer was removed using a surgical scalpel. The skin was incubated in trypsin-EDTA at 37°C for 35–45 min on an orbital shaker. A single-cell suspension was obtained by scraping the epidermal side and filtering. Cells were centrifuged for 8 min at 350 g at 4°C, resuspended in 5% fetal bovine serum, and stained for 30–40 min. The following antibodies were used: CD49f (Integrin alpha 6)-PE (eBioscience, 12–0495-82, 1:500), CD34-eFlour660 (eBioscience, 50–0341-82, 1:100), Sca-1-PerCP-Cy5.5 (eBioscience, 45–5981-82, 1:1000), and CD45-eFlour450 (eBioscience, 48–0451-82, 1:250). The HFSCs were isolated as $CD45^{-}$, Integrin alpha 6^{+}, $CD34^{+}$, $Sca\text{-}1^{-}$ cells, and the epidermal stem cells were isolated as $CD45^{-}$, Integrin alpha 6^{+}, $CD34^{-}$, $Sca\text{-}1^{+}$ cells, as described previously[1,17]. The data were analysed with FACSDiva (BD Biosciences, v8.0.2) and FlowJo (FlowJo LLC, v10.0.7).

RNA isolation

FACS-isolated cell populations were sorted directly into TRIzol LS Reagent (Thermo Fisher Scientific, Cat #10296028). RNA was isolated using an RNeasy Micro Kit (Qiagen, Cat#74004), using QIAcube according to the manufacturer's instructions. RNA concentration and RNA integrity were determined by Bioanalyzer (Agilent) using the RNA 6000 Pico kit (Agilent, Cat #5067–1513). High-quality RNA samples with RNA integrity number ≥ 8 were used as input for qRT-PCR and RNAseq.

Complementary DNA synthesis and quantitative real-time PCR

Complementary DNA was synthesized using the Superscript IV VILO Master Mix with ezDNase Enzyme (Thermo Fisher Scientific, Cat #11766050). Quantitative real-time PCR was performed using power SYBR Green dye (Thermo Fisher Scientific, Cat #4368706) on a QuantStudio 6 Flex Real-Time PCR system. Ct values were normalized to an internal control (*beta-actin*).

RNA-sequencing and computational analysis

RNA-sequencing libraries were prepared using 1 ng of total RNA as input. A SMART-Seq v4 Ultra Low Input RNA Kit for Sequencing (Takara, 634888) was used for

cDNA synthesis, with a 10-cycle PCR enrichment. Sequencing libraries were made using Illumina's Nextera XT Library Prep kit (Illumina, FC-131–1024). Single-read sequencing reads for DP samples were obtained using the Illumina NextSeq 500 platform, and aligned to the mouse reference genome (mm10) using Salmon (v1.55)[49]. Paired-end sequencing reads for HFSC samples were trimmed with Trim Galore! (v0.4.1, https://www.bioinformatics.babraham.ac.uk/projects/tr-im_galore/) and aligned to mm10 using STAR (v2.5.3)[50]. The reads were annotated using featurecounts[51]. Differential expression analysis was performed using the DESeq2 package (v1.22.2) in R (v3.5.1) and RStudio (v1.1.453)[52]. Gene Ontology (GO) enrichment analysis was performed using the database for annotation, visualization and integrated discovery (DAVID) web-accessible tool (v6.8) [53,54]. Transcripts Per Kilobase Million (TPM) calculated from counts of control HFSC samples were used to determine the expression levels of *Axl* receptor shown in Extended Data Fig. 8g. Signal peptide prediction and secretome analysis were performed on differentially expressed genes (DEGs) using the Phobius web-accessible tool (https://phobius.sbc.su.se/)[55] and the secretome knowledge base available at the MetazSecKB web-accessible tool[56].

Colony formation assay

FACS-purified HFSCs were plated on mitomycin C (P212121, Cat #M92010)-treated J2 fibroblast feeders at a density of 10,000 cells/well in12-well plates in E media supplemented with 15% (v/v) serum and 0.3 mM calcium as described in previous studies[57]. For GAS6 treatment, E medium was supplemented with recombinant mouse GAS6 protein (R&D systems, Cat #8310-GS) at 500 ng/ml. For R428-treatment experiments, E medium was supplemented with R428 (APExBIO, Cat #A8329) at 1 μM. Cells were fixed and stained with 1% (wt/vol) Rhodamine B (Millipore Sigma, R6626). Colony diameter was measured from scanned images of plates using ImageJ (v1.52h).

Imaging and image analysis

Images were obtained with a Zeiss LSM 880 confocal microscope with a 20x air objective or 40x oil-based objective (Carl Zeiss) or a Keyence BX-700 epifluorescence microscope with x4, x20 or x40 objective (Keyence). Images are presented as maximum intensity projection images or a single Z stack. Images were further processed and assembled into panels using Adobe Photoshop (v.21.2.4) and Adobe Illustrator (v.24.3).

Statistical analyses

Statistical analyses were performed with GraphPad Prism v8.4.2 (GraphPad Software) with unpaired two-sided Student's t-test, one-way ANOVA with Tukey's two-sided multiple comparisons, two-way ANOVA with Bonferroni's two-sided multiple comparisons, or two-way repeated measures ANOVA with Bonferroni's two-sided multiple comparisons. The DESeq2 package utilized the Wald test for hypothesis testing and the Benjamini–Hochberg method for multiple testing correction, and genes were considered differentially expressed with an adjusted p-value below 0.05. DAVID utilized one-sided Fisher's exact test with FDR correction. The data are presented as mean ± S.E.M. No statistical methods were used to predetermine sample size.

Statistics and Reproducibility

Figure 1a, n = 5 mice per condition. The experiments were performed three times with similar results. Two-way repeated measures ANOVA with Bonferroni's two-sided multiple comparisons. b, n = 20 HFs from 4 mice per condition. The experiments were performed three times with similar results. Two-way ANOVA with Bonferroni's two-sided multiple comparisons. c, n = 30 HFs from 5 mice per condition. The experiments were performed three times with similar results. Two-way ANOVA with Bonferroni's two-sided multiple comparisons. d, n = 5 mice per condition. The experiments were performed twice with similar results. Two-way ANOVA with Bonferroni's two-sided multiple comparisons. e, n = 7 (sham), n = 6 (ADX) mice. The experiments were performed twice with similar results. Two-way repeated measures ANOVA with Bonferroni's two-sided multiple comparisons. f, n = 5 mice per condition. The experiments were performed twice with similar results.

Figure 2a, n = 3 mice per condition. The experiments were performed three times with similar results. One-way ANOVA with Tukey's two-sided multiple comparisons test. b, Left, n = 5 mice per condition. The experiments were performed three times with similar results. Two-way repeated measures ANOVA with Bonferroni's two-sided multiple comparisons. Right, the experiments were performed three times with similar results. c, n = 5 mice per condition. The experiments were performed three times with similar results. Two-way repeated measures ANOVA with Bonferroni's two-sided multiple comparisons. d, n = 10 mice per condition. The experiments were performed three times with similar results. Two-way repeated measures ANOVA with Bonferroni's two-sided multiple comparisons.

Figure 3a, n = 3 biologically independent samples per condition. The experiments were performed twice with similar results. Two-sided unpaired t-test. b, n = 6 mice per condition. The experiments were performed three times with similar results. Two-way repeated measures ANOVA with Bonferroni's two-sided multiple comparisons. c, The experiments were performed three times with similar results. d, The experiments were performed three times with similar results. e, n = 5 mice per condition. The experiments were performed three times with similar results. g, n = 2 biological replicates from each condition. The experiments were performed once. One-sided Fisher's exact test with FDR correction.

Figure 4a, n = 20 HFs from 4 mice per condition. The experiments were performed three times with similar results. One-way ANOVA with Tukey's two-sided multiple comparisons test. b, n = 3 biologically independent samples per condition. The experiments were performed three times with similar results. Two-sided unpaired t-test. c, Left, n = 5 mice per condition. The experiments were performed three times with similar results. Right, the experiments were performed three times with similar results. d, n = 5 mice per condition. The experiments were performed three times with similar results.

Extended Data Figure 1a, The experiments were performed three times with similar results. b, n = 5 mice per condition. The experiments were performed three times with similar results. Two-way repeated measures ANOVA with Bonferroni's two-sided multiple comparisons. d, n = 20 HFs from 4 mice per condition. The experiments were performed three times with similar results. Two-sided unpaired t-test. e, n = 20 HFs (guard hairs), n = 30 HFs (awl/auchene hairs and zigzag hairs) from 4 mice per condition. The

experiments were performed three times with similar results. Two-sided unpaired *t*-test. f, The experiments were performed three times with similar results. g, The experiments were performed three times with similar results. h, *n* = 30 HFs from 5 mice per condition. The experiments were performed three times with similar results. Two-sided unpaired *t*-test. i, *n* = 30 skin regions from 5 mice per condition. The experiments were performed three times with similar results. Two-sided unpaired *t*-test. j, *n* = 7 (sham), *n* = 6 (ADX) mice. The experiments were performed twice with similar results. k, *n* = 5 mice per condition. The experiments were performed twice with similar results. Two-sided unpaired *t*-test. l, *n* = 40 skin regions from 4 mice per condition. The experiments were performed twice with similar results. One-way ANOVA with Tukey's two-sided multiple comparisons.

Extended Data Figure 2a, The experiments were performed three times with similar results. b, *n* = 114, 127, 100 HFs from 3 mice (sham), *n* = 100, 100, 119 HFs from 3 mice (ADX). The experiments were performed twice with similar results. Two-sided unpaired *t*-test. c, Left, *n* = 20 HFs from 4 mice per condition. The experiments were performed three times with similar results. Right, *n* = 2 biological independent samples per condition. The experiments were performed twice with similar results. d, *n* = 3 mice per condition. The experiments were performed three times with similar results. Two-sided unpaired *t*-test. e, *n* = 3 mice per condition. The experiments were performed twice with similar results. Two-sided unpaired *t*-test. f, *n* = 5 mice per condition. The experiments were performed twice with similar results. Two-way ANOVA repeated measures with Bonferroni's two-sided multiple comparisons. g, *n* = 3 mice. The experiments were performed three times with similar results. Two-sided unpaired *t*-test. h, *n* = 5 mice per condition. The experiments were performed twice with similar results. Two-sided unpaired *t*-test. i, *n* = 5 mice per condition. The experiments were performed three times with similar results. Two-way ANOVA repeated measures with Bonferroni's two-sided multiple comparisons. j, *n* = 5 mice per condition. The experiments were performed twice with similar results. Two-way ANOVA repeated measures with Bonferroni's two-sided multiple comparisons. k, *n* = 30 skin regions from 3 mice per condition. The experiments were performed three times with similar results. Two-sided unpaired *t*-test. l, The experiments were performed three times with similar results. m, *n* = 4 mice (Vehicle), *n* = 5 mice (CORT). The experiments were performed twice with similar results. Two-way ANOVA repeated measures with Bonferroni's two-sided multiple comparisons.

Extended Data Figure 3a, *n* = 3 mice per condition. The experiments were performed three times with similar results. Two-sided unpaired *t*-test. b, The experiments were performed three times with similar results. c, The experiments were performed three times with similar results. d, *n* = 5 mice per condition. The experiments were performed three times with similar results. Two-way repeated measures ANOVA with Bonferroni's two-sided multiple comparisons. e, *n* = 4 mice per condition. The experiments were performed three times with similar results. One-way ANOVA with Tukey's two-sided multiple comparisons. f, *n* = 5 mice (sham), *n* = 7 mice (ADX). The experiments were performed three times with similar results. Two-way repeated measures ANOVA with Bonferroni's two-sided multiple comparisons.

Extended Data Figure 4a. Top, $n = 3$ biologically independent samples per condition. The experiments were performed twice with similar results. Two-sided unpaired *t*-test. Bottom, the experiments were performed three times with similar results. b, $n = 5$ mice per condition. The experiments were performed three times with similar results. Two-way repeated measures ANOVA with Bonferroni's two-sided multiple comparisons. c, The experiments were performed three times with similar results. d, $n = 20$ HFs from 4 mice per condition. The experiments were performed three times with similar results. Two-way ANOVA with Bonferroni's two-sided multiple comparisons. e, $n = 30$ HFs from 5 mice per condition. The experiments were performed three times with similar results. Two-way ANOVA with Bonferroni's two-sided multiple comparisons. f, $n = 5$ mice per condition. The experiments were performed twice with similar results. Two-way repeated measures ANOVA with Bonferroni's two-sided multiple comparisons. g, $n = 30$ HFs from 5 mice per condition. The experiments were performed three times with similar results. Two-sided unpaired *t*-test. h, $n = 30$ skin regions from 5 mice per condition. The experiments were performed three times with similar results. Two-sided unpaired *t*-test.

Extended Data Figure 5a. $n = 2$ biological independent samples per condition. The experiments were performed twice with similar results. b, $n = 118, 139, 149$ HFs per mouse from 3 mice. The experiments were performed three times with similar results. Two-sided unpaired *t*-test. c, The experiments were performed three times with similar results. d, $n = 3$ mice per condition. The experiments were performed twice with similar results. Two-way repeated measures ANOVA with Bonferroni's two-sided multiple comparisons test. e, $n = 20$ guard HFs from 4 mice per condition. The experiments were performed three times with similar results. Two-sided unpaired *t*-test. f, $n = 20$ guard HFs from 4 mice per condition. The experiments were performed three times with similar results. Two-sided unpaired *t*-test. g, $n = 20$ guard HFs from 4 mice per condition. The experiments were performed three times with similar results. Two-sided unpaired *t*-test.

Extended Data Figure 6a–d, $n = 2$ biological independent samples for each condition. The experiments were performed once. e, $n = 4$ biological independent samples per condition. The experiments were performed twice with similar results. Two-sided unpaired *t*-test. f, $n = 3$ biological independent samples per condition. The experiments were performed twice with similar results. Two-sided unpaired *t*-test.

Extended Data Figure 7a,b, $n = 3$ biological independent samples per condition. The experiments were performed twice with similar results. Two-sided unpaired *t*-test. c,d, $n = 4$ biological independent samples per condition. The experiments were performed twice with similar results. Two-sided unpaired *t*-test. f,g, The experiments were performed three times with similar results. h, $n = 3$ biological independent samples. The experiments were performed once. i,j $n = 2$ biological independent samples for each condition. The experiments were performed once.

Extended Data Figure 8a, $n = 2$ biological independent samples for each condition. The experiments were performed once. b,c, $n = 2$ biological independent samples for each condition. The experiments were performed once. Two-sided Wald test with multiple testing adjustments using the Benjamini–Hochberg method in DESeq2. d, $n = 20$ HFs from 4 mice

per condition. The experiments were performed three times with similar results. Two-way ANOVA with Bonferroni's two-sided multiple comparisons. e, Top, the experiments were performed three times with similar results. Bottom, $n = 4$ biological independent samples per condition. The experiments were performed twice with similar results. Two-sided unpaired *t*-test. f, The experiments were performed three times with similar results. g, $n = 2$ biological independent samples per condition. The experiments were performed once. h, $n = 3$ biological independent samples per condition. The experiments were performed three times with similar results. One-way ANOVA with Tukey's two-sided multiple comparisons.

Extended Data Figure 9a, The experiments were performed four times with similar results. b, $n = 2$ biologically independent samples per condition. The experiments were performed twice with similar results. c, $n = 20$ HFs from 4 mice per condition. The experiments were performed three times with similar results. Two-way ANOVA with Bonferroni's two-sided multiple comparisons. d, $n = 30$ HFs from 5 mice per condition. The experiments were performed three times with similar results. Two-way ANOVA with Bonferroni's two-sided multiple comparisons. e, $n = 20$ HFs from 4 mice per condition. The experiments were performed three times with similar results. Two-sided unpaired *t*-test. f, $n = 30$ HFs from 5 mice per condition. The experiments were performed three times with similar results. Two-sided unpaired *t*-test. g, $n = 30$ skin regions from 5 mice per condition. The experiments were performed three times with similar results. Two-sided unpaired *t*-test. h, $n = 3$ biologically independent samples per condition. The experiments were performed twice with similar results. Two-sided unpaired *t*-test. i, $n = 5$ mice per condition. The experiments were performed three times with similar results. Two-way repeated measures ANOVA with Bonferroni's two-sided multiple comparisons. j, $n = 3$ (sham+EtOH), $n = 4$ (ADX+EtOH), and $n = 4$ biologically independent samples (ADX+EtOH). The experiments were performed twice with similar results. Two-sided unpaired *t*-test.

Extended Data Figure 10a, $n = 20$ HFs from 4 mice per condition. The experiments were performed three times with similar results. One-way ANOVA with Tukey's two-sided multiple comparisons. b, $n = 3$ biologically independent samples per condition. The experiments were performed twice with similar results. Two-sided unpaired *t*-test. c, $n = 5$ per condition. The experiments were performed three times with similar results. Two-way ANOVA repeated measures with Bonferroni's two-sided multiple comparisons. d, $n = 5$ mice per condition. The experiments were performed twice with similar results. Two-sided unpaired *t*-test. e, $n = 3$ biologically independent samples per condition (left), $n = 4$ biologically independent samples per condition (right). The experiments were performed twice with similar results. Two-sided unpaired *t*-test. f, $n = 20$ HFs from 4 mice per condition. The experiments were performed three times with similar results. Two-sided unpaired *t*-test.

Data availability

The sequencing data that support the findings of this study have been deposited in the Gene Expression Omnibus (GEO) with the accession code GSE135705. DAVID web-accessible tool (v6.8) is available at https://david.ncifcrf.gov/. MetazSecKB web-accessible tool is

available at proteomics.ysu.edu/secretomes/animal/. Source data for all main figures and Extended Data figures are provided with the paper.

Extended Data

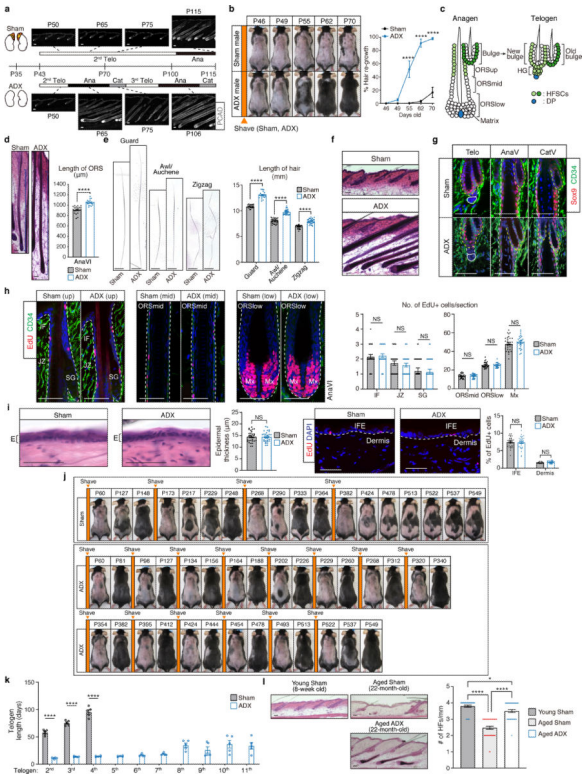

Extended Data Fig. 1 |. Hair cycle progression in ADX mice over time.

a, Hair cycle with immunohistochemical analyses (PCAD) in sham and ADX mice. **b**, Hair cycle progression in sham males and ADX males. **c**, Schematic depicting HFSCs in anagen and telogen. The upper ORS of anagen HFs contributes to the new bulge and hair germ (HG) of the following telogen HFs. See Ref[14,15] for details. **d**, The ORS length in the zigzag hairs of sham (P113) and ADX mice (P65) during late anagen. Brackets: the ORS length below the bulge. **e**, The hair shaft length of each hair subtype in sham and ADX mice after anagen. **f**, H&E staining at P65 of sham and ADX skin. **g**, Immunohistochemical analyses (Sox9 and CD34) in telogen (telo), late anagen (AnaV), and mid-catgen (CatV) HFs. Yellow dashed lines: bulge; white dashed lines: HG (telo), HF (AnaV, CatV); solid line: DP. **h**, Immunocolocalization (EdU and CD34) in infundibulum (IF), junctional zone (JZ), sebaceous gland (SG), mid ORS (ORS^{mid}), lower ORS (ORS^{low}), and matrix (Mx) of late anagen (AnaVI) HFs. Dashed lines: HF. **i**, H&E staining in the late anagen skin of sham and ADX mice with quantification of the epidermal thickness (E) (left). Immunocolocalization (EdU and DAPI) in interfollicular epidermis (IFE) and dermis (right). Dashed lines: the boundary between epidermis and dermis. **j**, Representative hair re-growth status of sham and ADX mice from P60 to P549. **k**, Telogen duration of sham and ADX mice. **l**, H&E staining of young sham, aged sham, and aged ADX mice with quantification of HF number per mm. Yellow dashed lines: bulge; White dashed lines: HG, Solid lines: DP. Telo, telogen; Ana,

anagen; Cat, Catagen. Scale bars, 50 μm (**a**,**d**,**f**,**g**,**h**,**i**,**l**), 1 mm (**e**). Data are mean±s.e.m. *P < 0.05, ****P < 0.0001, NS, not significant. Exact P values see source data files. Statistics, sample sizes, and numbers of replications are in Methods, 'Statistics and Reproducibility'.

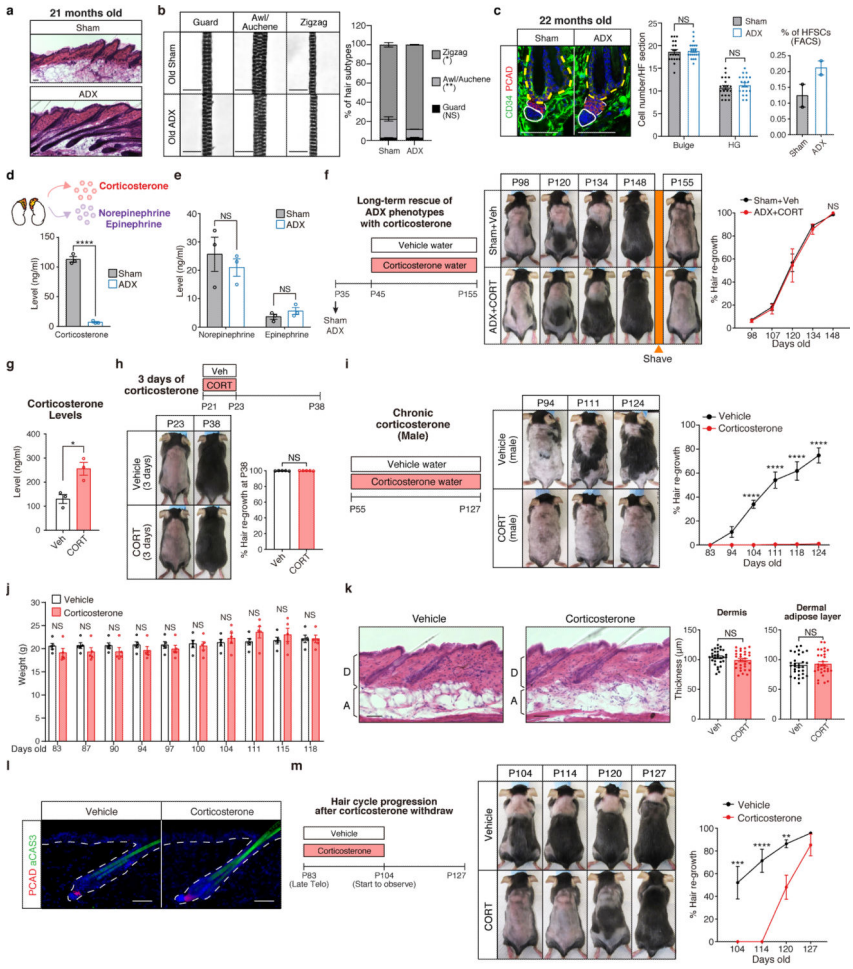

Extended Data Fig. 2 |. Corticosterone restores normal hair cycle progression in ADX mice. **a**, H&E staining of 21-month-old sham and ADX skin. **b**, Morphology of each hair subtype from skin of 18-month-old sham and ADX mice. **c**, Immunohistochemical analyses (CD34 and PCAD) of telogen HF in sham and ADX skin at 22 months old showing normal HF morphology and comparable stem cell numbers. Quantification of the number of bulge and hair germ cells per HF left). Quantification of % of HFSCs in epithelial fraction by FACS (right). **d**, Hormones from the adrenal gland and plasma levels of corticosterone in P45 sham and ADX animals. **e**, Plasma levels of norepinephrine and epinephrine measured by LC-MS/MS at P45 (10 days after surgery) in sham and ADX mice. **f**, Experimental design to test if supplying corticosterone rescues ADX phenotypes (left). Hair cycle progression of sham fed with vehicle (sham+Veh) or ADX fed with corticosterone (ADX+CORT) (right). **g**, Plasma corticosterone levels at P62 in C57BL/6 mice after a week's feeding with vehicle or corticosterone. **h**, Experimental design for 3 days of corticosterone feeding (top). Quantification shows % of hair re-growth of the back skin at P38 (bottom). **i**, Hair cycle progression of C57BL/6 male mice fed with vehicle or corticosterone. Corticosterone

feeding prolonged telogen as long as corticosterone was provided to the mice (both male and female). **j**, Body weight in C57BL/6 mice fed with vehicle or corticosterone from P83 to P118. **k**, H&E staining in the skin of vehicle and corticosterone-fed mice (left). Quantification of the thickness of dermis (middle) and dermal adipose layer (right). D, dermis; A, adipose layer. **l**, Immunohistochemical analysis (active caspase 3 (aCAS3) and PCAD) in vehicle- and corticosterone-fed mice. Dashed lines: epidermis and HFs. **m,** Experimental design to test effect of corticosterone withdrawal (left). Hair cycle progression of C57BL/6 mice after completion of 3 weeks of vehicle or corticosterone feeding (right). Veh, vehicle; CORT, corticosterone. Scale bars, 50 μm (**a**,**b**,**c**,**k,l**). Data are mean±s.e.m. *P < 0.05, **P < 0.01, ***P < 0.001, ****P < 0.0001, NS, not significant. Exact P values see source data files. Statistics, sample sizes, and numbers of replications are in Methods, 'Statistics and Reproducibility'.

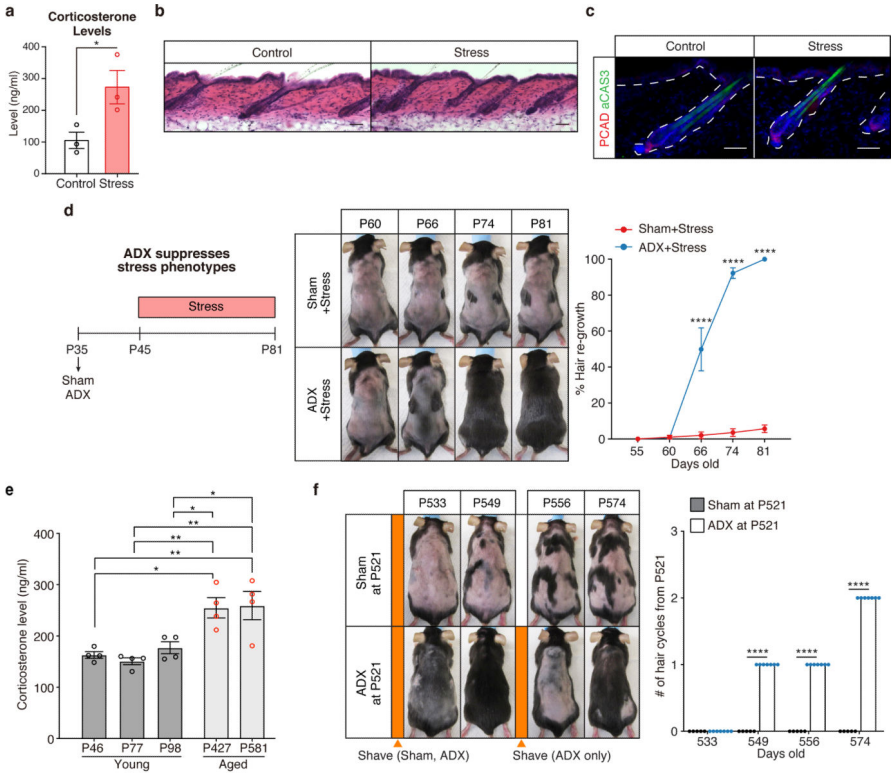

Extended Data Fig. 3 |. Removal of the adrenal glands in stressed or aged mice leads to hair follicle regeneration.

a, Plasma corticosterone levels at P62 in non-stressed control and stressed mice. **b**, **c**, H&E staining (**b**) and immunohistochemical analyses (active caspase3 (aCAS3) and PCAD) (**c**) in control and stressed mice. Dashed lines, epidermis and HFs. **d,** Stressed sham (sham+Stress) and stressed ADX (ADX+Stress) mice were monitored for hair coat recovery. Quantification shows % of back skin covered by newly regenerated hairs. **e**, Plasma levels of corticosterone in young mice (P46, P77, and P98) and aged mice (P427 and P581). **f**, Sham and ADX operations were performed on aged mice (P521). The mice were shaved and monitored for hair coat recovery from P521 to P574. Scale bars, 50 μm (**b**,**c**). Data are mean±s.e.m. *P <

0.05, $^{**}P < 0.01$, $^{****}P < 0.0001$. Exact *P* values see source data files. Statistics, sample sizes, and numbers of replications are in Methods, 'Statistics and Reproducibility'.

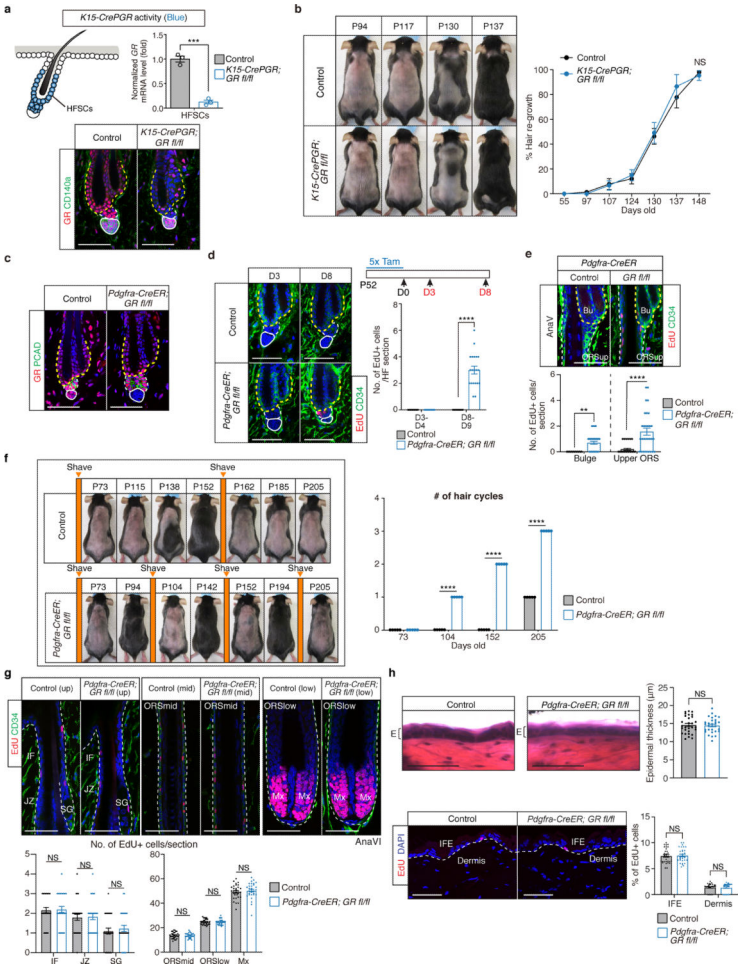

Extended Data Fig. 4. GR depletion in different cell types in the skin.

a, *K15-CrePGR* depletes GR efficiently in HFSCs (top). Immunohistochemical analysis (GR and CD140a) of telogen HF in control and *K15-CrePGR;GRfl/fl* skin (bottom). **b**, Hair cycle progression of control and *K15-CrePGR;GRfl/fl* mice. **c**, *Pdgfra-CreER* depletes GR efficiently in the dermis. Immunohistochemical analyses (GR and PCAD) of telogen HF in control and *Pdgfra-CreER;GRfl/fl* skin. **d**, Premature HFSC activation in *Pdgfra-CreER;GRfl/fl* as revealed by EdU incorporation. Immunocolocalization (EdU and CD34) in control and *Pdgfra-CreER;GRfl/fl* HFs after tamoxifen administration. **e**, Comparison of EdU localization in bulge and upper outer root sheath (ORS) in late anagen (AnaV) of control (P124) and *Pdgfra-CreER;GRfl/fl* mice (P73). **f**, Representative hair regeneration status of control and *Pdgfra-CreER;GRfl/fl* mice from P73 to P205 with the quantification of the hair cycle numbers. **g**, Immunocolocalization (EdU and CD34) in infundibulum (IF), junctional zone (JZ), sebaceous gland (SG), mid ORS (ORS^{mid}), lower ORS (ORS^{low}), and matrix (Mx) of late anagen (AnaVI) HFs in control and *Pdgfra-CreER;GRfl/fl* mice during late anagen with quantifications. **h**, H&E staining in the late anagen skin of control and *Pdgfra-CreER;GRfl/fl* with quantification of the thickness of epidermis (E) (top).

Immunocolocalization (EdU and DAPI) in interfollicular epidermis (IFE) and dermis in control and *Pdgfra-CreER;GRfl/fl* mice (bottom). Scale bars, 50 μm (**a**,**c**,**d**,**e**,**g**,**h**). Yellow dashed lines, bulge (**a**,**c**,**d**,**e**); white dashed lines, hair germ (**a**,**c**,**d**), the rest of hair follicles (**e**,**g**), or the boundary between epidermis and dermis (**h**); solid white line, dermal papilla (DP) (**a**,**c**,**d**). Data are mean±s.e.m. $^{**}P < 0.01$, $^{***}P < 0.001$, $^{****}P < 0.0001$, NS, not significant. Exact *P* values see source data files. Statistics, sample sizes, and numbers of replications are in Methods, 'Statistics and Reproducibility'.

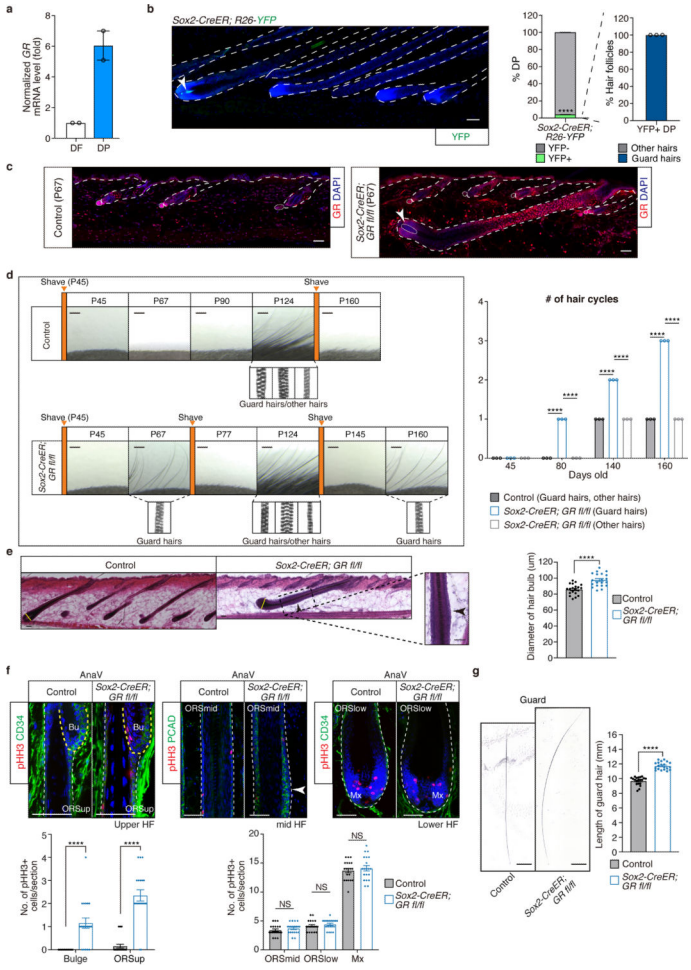

Extended Data Fig. 5. Corticosterone acts on dermal papilla.

a, qRT-PCR of *GR* from dermal papilla (DP) and dermal fibroblasts (DF). **b**, Immunohistochemical analyses (YFP and DAPI) of anagen *Sox2-CreER;R26-lsl-YFP* skin. Arrowhead: an anagen guard hair follicle with YFP^{+ve} DP cells (left). Quantification of the percentage of YFP^{+ve} and YFP^{-ve} DP in *Sox2-CreER;R26-lsl-YFP*. Only guard hair follicles have YFP^{+ve} DP (right). **c**, Immunohistochemical analyses (GR and DAPI) of control and *Sox2-CreER;GRfl/fl* skin. Dashed lines: epidermis and hair follicles; solid line: DP. Arrowhead: DP of *Sox2-CreER;GRfl/fl* guard hairs. **d**, Representative hair regeneration status of control and *Sox2-CreER; GR fl/fl* mice from P45 to P160. Quantification showing the hair cycle numbers for guard hairs and other hairs in control and *Sox2-CreER; GR fl/fl* mice. **e**, Comparison of the hair bulb diameter in late anagen (AnaV) control (P120)

and *Sox2-CreER;GRfl/fl* skin (P67). Yellow lines: hair bulb diameter. Arrowhead denotes minor hyper-thickening of *Sox2-CreER; GR fl/fl* hair follicle around the ORS, likely because the dermis has not expanded to accommodate the extra proliferation from HFSCs. **f**, Immunocolocalization of phospho-Histone H3 (pHH3) and CD34 in bulge and upper ORS, middle ORS (ORS^{mid}), lower ORS (ORS^{low}), and matrix (Mx) of late anagen (AnaV) guard HFs in control and *Sox2-CreER;GRfl/fl* mice. White arrowhead denotes thickened region in *Sox2-CreER; GR fl/fl* hair follicle, likely due to excessive proliferation from HFSCs. Yellow dashed lines, bulge; white dashed lines, the rest of hair follicles. **g**, Hair shaft length of guard hairs in control and *Sox2-CreER;GRfl/fl* mice after anagen. Scale bars, 50 μm (**b**,**c**,**e**,**f**), 1 mm (**d**,**g**). Data are mean±s.e.m. ****$P < 0.0001$, NS, not significant. Exact P values see source data files. Statistics, sample sizes, and numbers of replications are in Methods, 'Statistics and Reproducibility'.

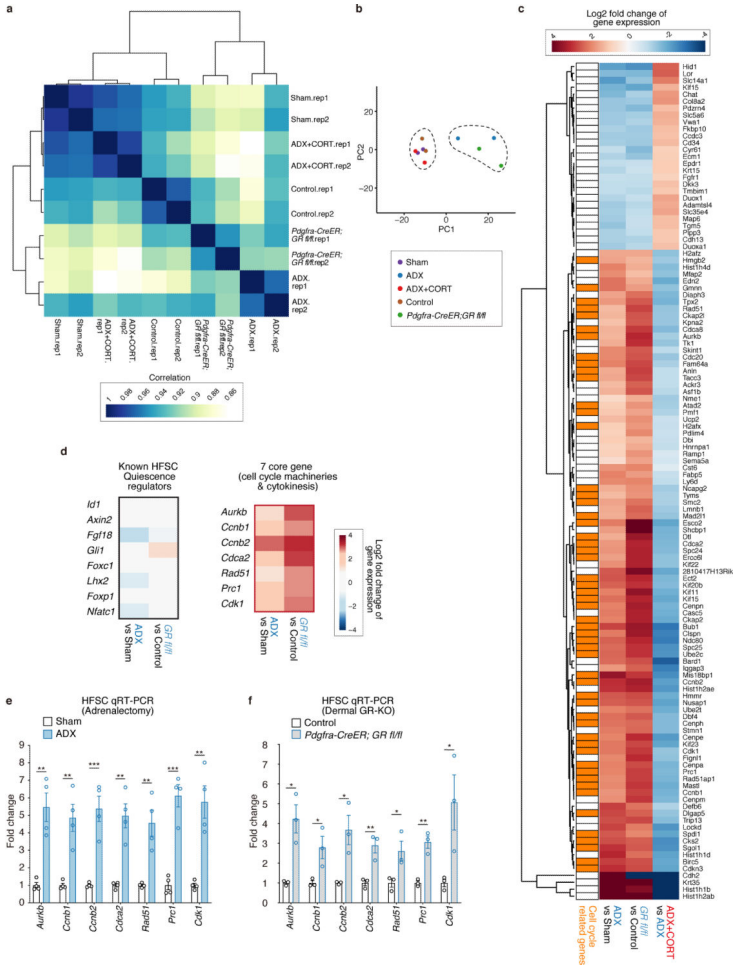

Extended Data Fig. 6 |. Differential gene expression in HFSCs of control, ADX, and dermal GR knockout mice.

a, Sample clustering based on Pearson's correlation of transcriptomes in sham, ADX, and ADX+CORT, as well as control and *Pdgfra-CreER;GRfl/fl* HFSCs. **b**, Principal component analysis (PCA) comparing the transcriptome of sham, ADX, ADX+CORT, control, and *Pdgfra-CreER;GRfl/fl* HFSCs. **c**, Heat map of log2 fold change of gene expression of 121

common genes among ADX (versus sham), *Pdgfra-CreER;GRfl/fl* (versus control), and ADX+CORT (versus ADX). Cell cycle-related genes are noted in orange. **d**, (Left) heat map of log2 fold change of gene expression of transcription factors (*Foxc1, Lhx2, Foxp1, Nfatc1*), key signalling factors (*Fgf18*), or downstream readout of key signalling factors (*Id1* for BMP pathway, *Axin2* for WNT pathway, *Gli1* for SHH pathway) known to regulate HFSC quiescence. (Right) heat map of log2 fold change of gene expression of 7 core genes related to cell cycle machineries and cytokinesis. **e**, **f**, qRT-PCR of genes related to cell cycle machineries and cytokinesis from telogen HFSCs of sham and ADX mice (**e**) and control and *Pdgfra-CreER;GRfl/fl* mice (**f**). Data are mean±s.e.m. *$P < 0.05$, **$P < 0.01$, ***$P < 0.001$. Exact P values see source data files. Statistics, sample sizes, and numbers of replications are in Methods, 'Statistics and Reproducibility'.

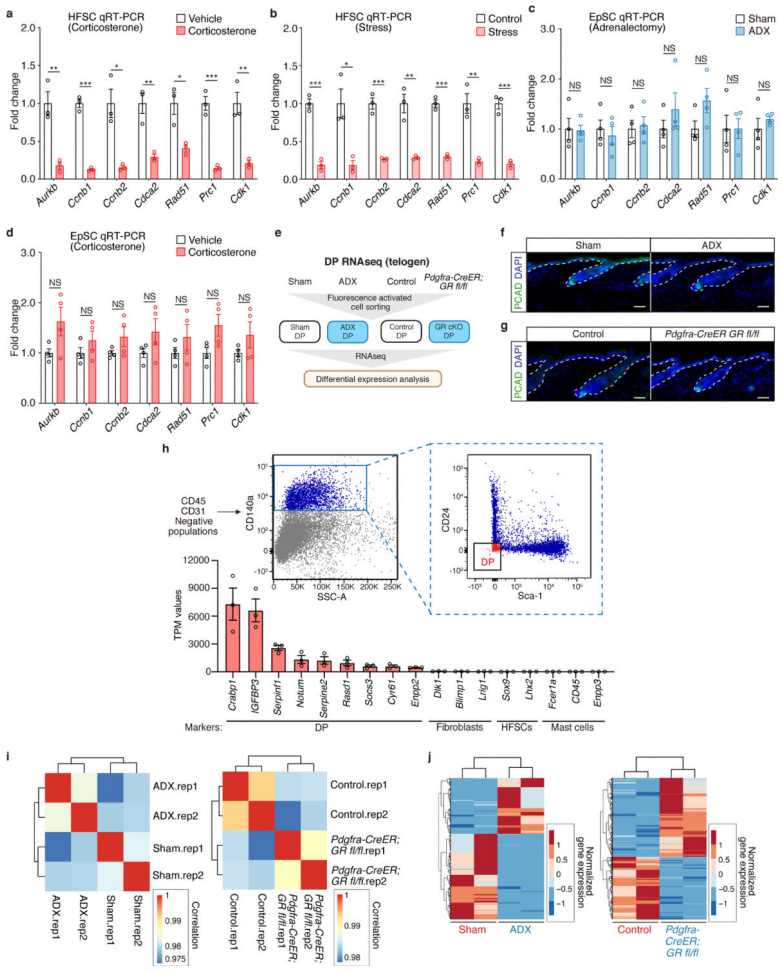

Extended Data Fig. 7 |. The expression of cell cycle-related genes in HFSCs.

a, b, qRT-PCR of genes related to cell cycle machineries and cytokinesis using telogen HFSCs from vehicle and corticosterone-fed mice (**a**) and control and stressed mice (**b**). **c**, **d**, qRT-PCR of genes related to cell cycle machineries and cytokinesis in telogen epidermis from sham and ADX mice (**c**) and vehicle and corticosterone fed mice (**d**). **e**, Experimental workflow of the differentially expressed genes (DEGs, > 1.5 fold, adjusted $P < 0.05$) from DP cells of sham and ADX mice, as well as control and *Pdgfra-CreER;GRfl/fl* mice. **f,**

g, Immunohistochemical analysis (PCAD) of skin samples from sham and ADX (**f**) or control and *Pdgfra-CreER GR fl/fl* (**g**) used in RNAseq experiments to validate hair cycle (all telogen). Dashed lines, epidermis and HFs. **h**, FACS strategies for isolating DP cells for RNAseq[24,44] (top). The expression levels of cell type-specific signature genes (DP, fibroblasts, HFSCs, and mast cells) in FACS-purified DP cells (bottom). TPM, transcripts per million. **i**, Sample clustering based on Pearson's correlation of transcriptomes in sham and ADX (left), as well as control and *Pdgfra-CreER;GRfl/fl* DPs (right). **j**, heatmaps of the differentially expressed genes (DEGs, > 1.5 fold, adjusted $P < 0.05$) from FACS-purified DP cells of sham and ADX mice (left) or control and *Pdgfra-CreER;GRfl/fl* mice (right). Scale bars, 50 μm (**f**,**g**). Data are mean±s.e.m. *$P < 0.05$, **$P < 0.01$, ***$P < 0.001$, NS, not significant. Exact P values see source data files. Statistics, sample sizes, and numbers of replications are in Methods, 'Statistics and Reproducibility'.

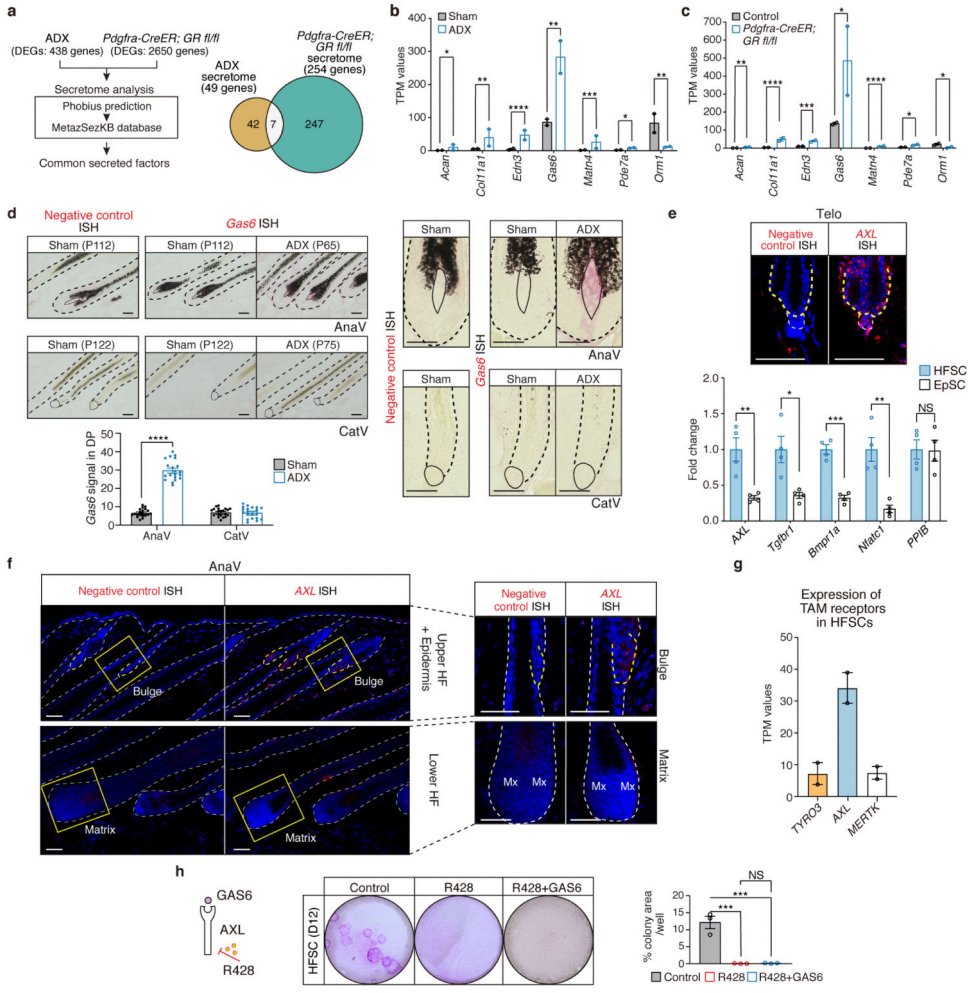

Extended Data Fig. 8 |. Transcriptome analysis and secretome analysis identified GAS6 as a secreted factor suppressed by systemic corticosterone in the DP.

a, Secretome analysis identifying common secreted factors from DEGs (> 1.5 fold, adjusted $P < 0.05$) in ADX and *Pdgfra-CreER;GRfl/fl* DP cells identified by RNAseq. **b**,**c**, Expression levels of shared differentially expressed secreted factors as transcripts per

million (TPM), in the DP cells of ADX (**b**) and *Pdgfra-CreER GR fl/fl* mice (**c**). **d**, Negative control and *Gas6* mRNA expression by *in situ* hybridization in late anagen (AnaV) and mid catagen (CatV) skin of sham and ADX mice. Quantification *Gas6* mRNA in the DP. Dashed lines, HF; solid lines, DP. **e**, Representative image of negative control and *Axl* mRNA expression by *in situ* hybridization in telogen skin. Yellow dashed lines: bulge; white dashed lines: hair germ (top). qRT-PCR of *Axl, Tgfbr1, Bmpr1a, Nfatc1* and *PPIB* from HFSCs and epidermal stem cells (EpSCs) of control mice (P83) (bottom). **f**, Representative images of negative control and *Axl* mRNA expression by *in situ* hybridization in late anagen skin. Yellow dashed lines: bulge; white dashed lines: epidermis and HFs. **g**, The expression levels as TPM of TAM receptors (*Tyro3*, *Axl*, and *Mertk*) in HFSCs. **h**, Schematic of the GAS6-AXL receptor tyrosine kinase pathway. R428 is a selective inhibitor of AXL tyrosine kinase activity[43] (left). Colony formation assays of cultured HFSCs in R428 or GAS6 with R428 with quantifications (right). Scale bars, 50 μm (**d**,**e**,**f**). Data are mean±s.e.m. *$P < 0.05$, **$P < 0.01$, ***$P < 0.001$, ****$P < 0.0001$, NS, not significant. Exact P values see source data files. Statistics, sample sizes, and numbers of replications are in Methods, 'Statistics and Reproducibility'.

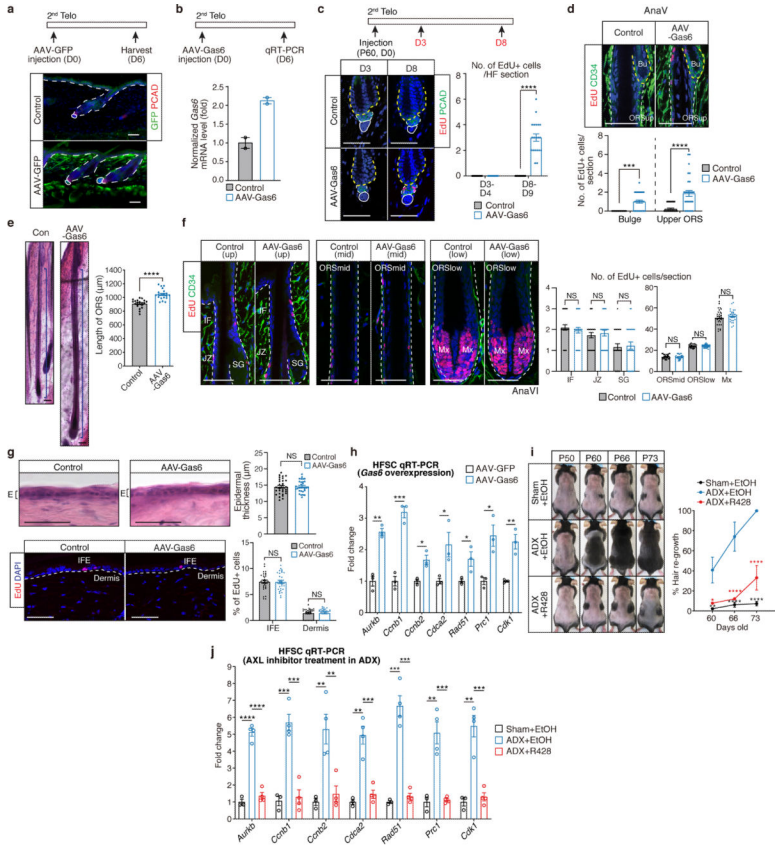

Extended Data Fig. 9 |. Analyses of skin changes upon *Gas6* overexpression or AXL inhibitor treatment.

a, Immunohistochemical analysis (GFP and PCAD) of PBS-injected 2nd telogen skin and AAV-GFP injected 2nd telogen skin. Dashed lines, epidermis and HFs; solid lines: DP. **b**, qRT-PCR of *Gas6* from dermal fibroblasts of PBS-injected 2nd telogen skin (control) and

AAV-Gas6 injected 2nd telogen skin. **c**, Precocious HFSC activation in mice injected with AAV-Gas6 shown by EdU incorporation. Immunocolocalization (EdU and CD34) in control and AAV-Gas6 injected skin after AAV injection (D3 to D9). **d**, Comparison of EdU and CD34 localization in bulge and upper outer root sheath (ORS) in late anagen (AnaV, control: D50 after injection; Gas6: D17 after injection). **e**, H&E staining of late anagen (AnaVI) skin (control: D53 after injection; Gas6: D20 after injection). Quantification of the ORS length in the zigzag hairs of control and AAV-Gas6 injected mice during late anagen. Brackets: the ORS length below the bulge. **f**, Immunocolocalization (EdU and CD34) in infundibulum (IF), junctional zone (JZ), sebaceous gland (SG), mid ORS (ORS^{mid}), lower ORS (ORS^{low}), and matrix (Mx) of late anagen (AnaVI) HFs in control and AAV-Gas6 injected mice with quantifications. Dashed lines, HFs. **g**, H&E staining in the late anagen skin of control and AAV-Gas6 injected mice with quantification of the thickness of epidermis (E) (top). Immunocolocalization (EdU and DAPI) in interfollicular epidermis (IFE) and dermis in control and AAV-Gas6 injected mice with quantifications (bottom). **h**, qRT-PCR of genes related to HFSC proliferation in HFSCs of 2nd telogen skin. **i**, Hair cycle progression of sham and ADX mice treated with ethanol topically, or ADX mice treated with R428 in ethanol. **j**, qRT-PCR of genes related to cell cycle machineries and cytokinesis from HFSCs of sham, ADX mice treated with ethanol topically, or ADX mice treated for 7 days with R428 (in ethanol) topically. Yellow dashed lines: bulge (**c**,**d**); white dashed lines: hair germ (**c**), the rest of the HF (**d**,**f**), or the boundary of epidermis and dermis (**g**); solid white line: DP (**c**). EtOH, ethonal. Scale bars, 50 μm (**a**,**c**,**d**,**e**,**f**,**g**). Data are mean±s.e.m. $*P < 0.05$, $**P < 0.01$, $***P < 0.001$, $****P < 0.0001$, NS, not significant. Exact *P* values see source data files. Statistics, sample sizes, and numbers of replications are in Methods, ‘Statistics and Reproducibility’.

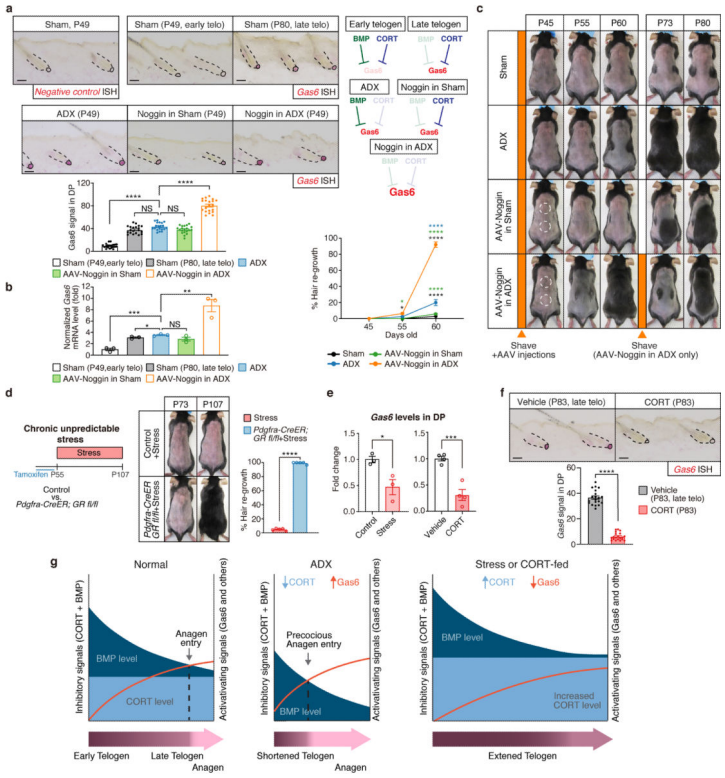

Extended Data Fig. 10 |. Interactions between systemic corticosterone and local BMP signalling.

a, *In situ* hybridization of negative control and *Gas6* mRNA expression in different conditions, including P49 (early telogen) of sham, P80 (late telogen) of sham, P49 of ADX alone, P49 of AAV-Noggin injection in sham mice (Noggin in sham), and P49 of AAV-Noggin injection in ADX mice (Noggin in ADX). Quantifications show *in situ* signal intensities in DP. Model denotes how changes in corticosterone and BMP signalling influence *Gas6* levels in DP. **b**, qRT-PCR of *Gas6* from DP of P49 (early telogen) and P80 (late telogen) of sham, and P49 of ADX, AAV-Noggin in sham, and AAV-Noggin in ADX mice. **c,** Hair cycle progression in sham, ADX, AAV-Noggin injection in sham, and AAV-Noggin injection in ADX with quantifications. Dashed circles: AAV-Noggin injection areas. **d**, Control and *Pdgfra-CreER;GRfl/fl* mice were subjected to chronic unpredictable stress from P55. Quantification shows % of hair re-growth at P107. **e**, qRT-PCR of *Gas6* from DP cells of control (P83) and stressed mice (P83) (left), and vehicle (P83) and corticosterone-fed mice (P83) (right). **f**, *In situ* hybridization of *Gas6* in vehicle (P83, late telogen) and corticosterone-fed mice (P83) with quantification of *in situ* signals in DP. **g,** Model for corticosterone regulation of telogen length. In normal conditions, corticosterone levels remain constant, but BMP levels naturally decrease as telogen progresses, until a point is reached at which *Gas6* levels are sufficiently elevated to drive HFSCs out of quiescence. This dynamic can be altered by changing either the corticosterone level or the BMP level. If corticosterone levels drop, the sum of inhibitory cues on *Gas6* drops below a critical threshold sooner in telogen, leading to elevated *Gas6* levels and precocious anagen entry. In the case of stress, age, or corticosterone feeding, elevated corticosterone levels reduce *Gas6* levels to below the critical threshold, leading to an extended telogen. Dashed lines, HFs; solid lines, DP. Scale bars, 50 μm (**a**,**f**). Data are mean±s.e.m. *$P < 0.05$, **$P < 0.01$, ***P

< 0.001, ****P < 0.0001, NS, not significant. Exact P values see source data files. Statistics, sample sizes, and numbers of replications are in Methods, ‘Statistics and Reproducibility’.

Supplementary Material

Refer to Web version on PubMed Central for supplementary material.

ACKNOWLEDGEMENTS

We thank many colleagues who generously donated mice to JAX; A. Regev, Y. Fong, and members of the Hsu laboratory, in particular Y. Shwartz, for helpful discussions and comments on the manuscript, and O. Chung for technical assistance; HCBI, HSCRB-HSCI FACS core, HSCRB Histology core, Small Molecule Mass Spectrometry Facility, Office of Animal Resources, and the Bauer Core Sequencing Facility at Harvard University for technical support. This work was supported in part by the New York Stem Cell Foundation (Y-C.H.); the Smith Family Foundation Odyssey Award (Y-C.H.); the Pew Charitable Trusts (Y-C.H.); Harvard Stem Cell Institute (Y-C.H. and A.S.); Harvard HMS Dean’s Award (Y-C.H.); American Cancer Society (Y-C.H.), James and Audrey Foster MGH Research Scholar Award (A.S.), NARSAD Young Investigator Award (A.B.), MGH ECOR Fund for Medical Discovery Postdoctoral Fellowship Awards (A.B.), New York State Department of Health (NYSTEM-C029574, NYSTEM-C32561GG to M.R.), NINDS (R56NS117529 to A.S.) and NIH (R01-AR070825 to Y.-C.H; R35-HL139598 to M.N.; R01MH104175, R01AG048908, 1R01MH111729 to A.S.; R01AR071047, R01AR063151 to M.R.). Y-C.H. is a New York Stem Cell Foundation – Robertson Investigator and a Pew Scholar. J.D.B. and S.M. acknowledge support from the Broad Institute Fellows Program.

REFERENCES

1. Shwartz Y et al. Cell Types Promoting Goosebumps Form a Niche to Regulate Hair Follicle Stem Cells. Cell 182, 578–593 e519 (2020). [PubMed: 32679029]
2. Lay K, Kume T & Fuchs E FOXC1 maintains the hair follicle stem cell niche and governs stem cell quiescence to preserve long-term tissue-regenerating potential. Proc Natl Acad Sci U S A 113, E1506–1515 (2016). [PubMed: 26912458]
3. Wang L, Siegenthaler JA, Dowell RD & Yi R Foxc1 reinforces quiescence in self-renewing hair follicle stem cells. Science 351, 613–617 (2016). [PubMed: 26912704]
4. Plikus MV et al. Cyclic dermal BMP signalling regulates stem cell activation during hair regeneration. Nature 451, 340–344 (2008). [PubMed: 18202659]
5. Muller-Rover S et al. A comprehensive guide for the accurate classification of murine hair follicles in distinct hair cycle stages. J Invest Dermatol 117, 3–15 (2001). [PubMed: 11442744]
6. Greco V et al. A two-step mechanism for stem cell activation during hair regeneration. Cell Stem Cell 4, 155–169 (2009). [PubMed: 19200804]
7. Hsu YC, Li L & Fuchs E Transit-amplifying cells orchestrate stem cell activity and tissue regeneration. Cell 157, 935–949 (2014). [PubMed: 24813615]
8. Sawaya ME & Hordinsky MK Glucocorticoid regulation of hair growth in alopecia areata. J Invest Dermatol 104, 30S (1995). [PubMed: 7738385]
9. Stenn KS, Paus R, Dutton T & Sarba B Glucocorticoid effect on hair growth initiation: a reconsideration. Skin Pharmacol 6, 125–134 (1993). [PubMed: 8352950]
10. Perez P et al. Altered skin development and impaired proliferative and inflammatory responses in transgenic mice overexpressing the glucocorticoid receptor. FASEB J 15, 2030–2032 (2001). [PubMed: 11511512]
11. Rose J & Sterner M The role of the adrenal glands in regulating onset of winter fur growth in mink (Mustela vison). J Exp Zool 262, 469–473 (1992). [PubMed: 1624919]
12. Butcher EO Hair growth in adrenalectomized, and, adrenalectomized thyroxin-treated rats. Am J Physiol 120, 427–434 (1937).
13. Whiteley HJ The effect of adrenalectomy and adrenocortical hormones on the hair growth cycle in the rabbit and rat. J Endocrinol 17, 167–176 (1958). [PubMed: 13563746]
14. Hsu YC, Pasolli HA & Fuchs E Dynamics between stem cells, niche, and progeny in the hair follicle. Cell 144, 92–105 (2011). [PubMed: 21215372]

15. Rompolas P, Mesa KR & Greco V Spatial organization within a niche as a determinant of stem-cell fate. Nature 502, 513–518 (2013). [PubMed: 24097351]
16. Chen CC et al. Regenerative hair waves in aging mice and extra-follicular modulators follistatin, dkk1, and sfrp4. J Invest Dermatol 134, 2086–2096 (2014). [PubMed: 24618599]
17. Keyes BE et al. Nfatc1 orchestrates aging in hair follicle stem cells. Proc Natl Acad Sci U S A 110, E4950–4959 (2013). [PubMed: 24282298]
18. Walczak EM & Hammer GD Regulation of the adrenocortical stem cell niche: implications for disease. Nat Rev Endocrinol 11, 14–28 (2015). [PubMed: 25287283]
19. Besnard A et al. Targeting Kruppel-like Factor 9 in Excitatory Neurons Protects against Chronic Stress-Induced Impairments in Dendritic Spines and Fear Responses. Cell Rep 23, 3183–3196 (2018). [PubMed: 29898391]
20. Heidt T et al. Chronic variable stress activates hematopoietic stem cells. Nat Med 20, 754–758 (2014). [PubMed: 24952646]
21. Tye KM et al. Dopamine neurons modulate neural encoding and expression of depression-related behaviour. Nature 493, 537–541 (2013). [PubMed: 23235822]
22. Enshell-Seijffers D, Lindon C, Kashiwagi M & Morgan BA beta-catenin activity in the dermal papilla regulates morphogenesis and regeneration of hair. Dev Cell 18, 633–642 (2010). [PubMed: 20412777]
23. Festa E et al. Adipocyte lineage cells contribute to the skin stem cell niche to drive hair cycling. Cell 146, 761–771 (2011). [PubMed: 21884937]
24. Zhang B et al. Hair follicles' transit-amplifying cells govern concurrent dermal adipocyte production through Sonic Hedgehog. Genes Dev 30, 2325–2338 (2016). [PubMed: 27807033]
25. Clavel C et al. Sox2 in the dermal papilla niche controls hair growth by fine-tuning BMP signaling in differentiating hair shaft progenitors. Dev Cell 23, 981–994 (2012). [PubMed: 23153495]
26. Driskell RR, Giangreco A, Jensen KB, Mulder KW & Watt FM Sox2-positive dermal papilla cells specify hair follicle type in mammalian epidermis. Development 136, 2815–2823 (2009). [PubMed: 19605494]
27. Horsley V, Aliprantis AO, Polak L, Glimcher LH & Fuchs E NFATc1 balances quiescence and proliferation of skin stem cells. Cell 132, 299–310 (2008). [PubMed: 18243104]
28. Rhee H, Polak L & Fuchs E Lhx2 maintains stem cell character in hair follicles. Science 312, 1946–1949 (2006). [PubMed: 16809539]
29. Leishman E et al. Foxp1 maintains hair follicle stem cell quiescence through regulation of Fgf18. Development 140, 3809–3818 (2013). [PubMed: 23946441]
30. Choi YS et al. Distinct functions for Wnt/beta-catenin in hair follicle stem cell proliferation and survival and interfollicular epidermal homeostasis. Cell Stem Cell 13, 720–733 (2013). [PubMed: 24315444]
31. Rothlin CV, Carrera-Silva EA, Bosurgi L & Ghosh S TAM receptor signaling in immune homeostasis. Annu Rev Immunol 33, 355–391 (2015). [PubMed: 25594431]
32. Wang Y et al. Axl-altered microRNAs regulate tumorigenicity and gefitinib resistance in lung cancer. Cell Death Dis 5, e1227 (2014). [PubMed: 24832599]
33. Asiedu MK et al. AXL induces epithelial-to-mesenchymal transition and regulates the function of breast cancer stem cells. Oncogene 33, 1316–1324 (2014). [PubMed: 23474758]
34. Balaji K et al. AXL Inhibition Suppresses the DNA Damage Response and Sensitizes Cells to PARP Inhibition in Multiple Cancers. Mol Cancer Res 15, 45–58 (2017). [PubMed: 27671334]
35. Aoki E, Shibasaki T & Kawana S Intermittent foot shock stress prolongs the telogen stage in the hair cycle of mice. Exp Dermatol 12, 371–377 (2003). [PubMed: 12930292]
36. Zhang B et al. Hyperactivation of sympathetic nerves drives depletion of melanocyte stem cells. Nature 577, 676–681 (2020). [PubMed: 31969699]
37. Arck PC et al. Stress inhibits hair growth in mice by induction of premature catagen development and deleterious perifollicular inflammatory events via neuropeptide substance P-dependent pathways. Am J Pathol 162, 803–814 (2003). [PubMed: 12598315]

38. Mittelstadt PR, Monteiro JP & Ashwell JD Thymocyte responsiveness to endogenous glucocorticoids is required for immunological fitness. The Journal of clinical investigation 122, 2384–2394 (2012). [PubMed: 22653054]
39. Morris RJ et al. Capturing and profiling adult hair follicle stem cells. Nat Biotechnol 22, 411–417 (2004). [PubMed: 15024388]
40. Kang SH, Fukaya M, Yang JK, Rothstein JD & Bergles DE NG2+ CNS glial progenitors remain committed to the oligodendrocyte lineage in postnatal life and following neurodegeneration. Neuron 68, 668–681 (2010). [PubMed: 21092857]
41. Arnold K et al. Sox2(+) adult stem and progenitor cells are important for tissue regeneration and survival of mice. Cell stem cell 9, 317–329 (2011). [PubMed: 21982232]
42. Srinivas S et al. Cre reporter strains produced by targeted insertion of EYFP and ECFP into the ROSA26 locus. BMC Dev Biol 1, 4 (2001). [PubMed: 11299042]
43. Holland SJ et al. R428, a selective small molecule inhibitor of Axl kinase, blocks tumor spread and prolongs survival in models of metastatic breast cancer. Cancer Res 70, 1544–1554 (2010). [PubMed: 20145120]
44. Goldstein JM et al. In Situ Modification of Tissue Stem and Progenitor Cell Genomes. Cell Rep 27, 1254–1264 e1257 (2019). [PubMed: 31018138]
45. Plikus MV & Chuong CM Complex hair cycle domain patterns and regenerative hair waves in living rodents. J Invest Dermatol 128, 1071–1080 (2008). [PubMed: 18094733]
46. Rezza A et al. Signaling Networks among Stem Cell Precursors, Transit-Amplifying Progenitors, and their Niche in Developing Hair Follicles. Cell Rep 14, 3001–3018 (2016). [PubMed: 27009580]
47. Rendl M, Lewis L & Fuchs E Molecular dissection of mesenchymal-epithelial interactions in the hair follicle. PLoS Biol 3, e331 (2005). [PubMed: 16162033]
48. Joost S et al. The Molecular Anatomy of Mouse Skin during Hair Growth and Rest. Cell Stem Cell 26, 441–457 e447 (2020). [PubMed: 32109378]
49. Patro R, Duggal G, Love MI, Irizarry RA & Kingsford C Salmon provides fast and bias-aware quantification of transcript expression. Nat Methods 14, 417–419 (2017). [PubMed: 28263959]
50. Dobin A et al. STAR: ultrafast universal RNA-seq aligner. Bioinformatics 29, 15–21 (2013). [PubMed: 23104886]
51. Liao Y, Smyth GK & Shi W featureCounts: an efficient general purpose program for assigning sequence reads to genomic features. Bioinformatics 30, 923–930 (2014). [PubMed: 24227677]
52. Love MI, Huber W & Anders S Moderated estimation of fold change and dispersion for RNA-seq data with DESeq2. Genome Biol 15, 550 (2014). [PubMed: 25516281]
53. Huang da W, Sherman BT & Lempicki RA Bioinformatics enrichment tools: paths toward the comprehensive functional analysis of large gene lists. Nucleic Acids Res 37, 1–13 (2009). [PubMed: 19033363]
54. Huang da W, Sherman BT & Lempicki RA Systematic and integrative analysis of large gene lists using DAVID bioinformatics resources. Nat Protoc 4, 44–57 (2009). [PubMed: 19131956]
55. Kall L, Krogh A & Sonnhammer EL A combined transmembrane topology and signal peptide prediction method. J Mol Biol 338, 1027–1036 (2004). [PubMed: 15111065]
56. Meinken J, Walker G, Cooper CR & Min XJ MetazSecKB: the human and animal secretome and subcellular proteome knowledgebase. Database (Oxford) 2015 (2015).
57. Nowak JA & Fuchs E Isolation and culture of epithelial stem cells. Methods in molecular biology 482, 215–232 (2009). [PubMed: 19089359]

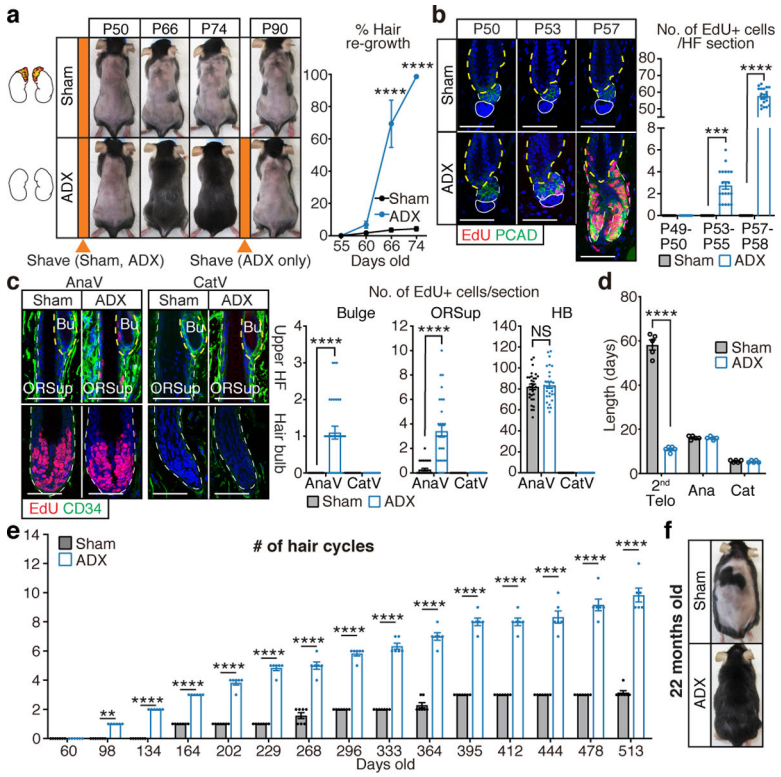

Fig. 1 |. Removal of adrenal glands activates HFSCs.

a, Sham and ADX mice were shaved and monitored for hair coat recovery. Quantifications show % of back skin covered by regrown hairs. **b**, EdU and PCAD staining in sham and ADX hair follicles (HFs) (P49 to P58) with quantifications. Yellow dashed lines: bulge; white dashed lines: hair germ or hair bulb (HB); solid lines: dermal papilla (DP). **c**, EdU and CD34 staining in late anagen (AnaV: sham, P110; ADX, P62) and catagen (CatV: sham, P122; ADX, P74). Yellow dashed lines: bulge (Bu); white dashed lines: rest of HF. ORS^{up} (upper outer root sheath) **d**, Hair cycle length. **e**, Hair cycle numbers of sham and ADX mice from P60 to P513 (see also Extended Data Fig. 1). **f,** Representative hair re-growth status of 22-month-old sham and ADX mice. Telo, telogen; Ana, anagen; Cat, Catagen. Scale bars, 50 μm (**b**,**c**). Data are mean±s.e.m. $^{**}P < 0.01$, $^{***}P < 0.001$, $^{****}P < 0.0001$, NS, not significant. Exact *P* values see source data files. Statistics, sample sizes, and numbers of replications are in Methods, ‘Statistics and Reproducibility’.

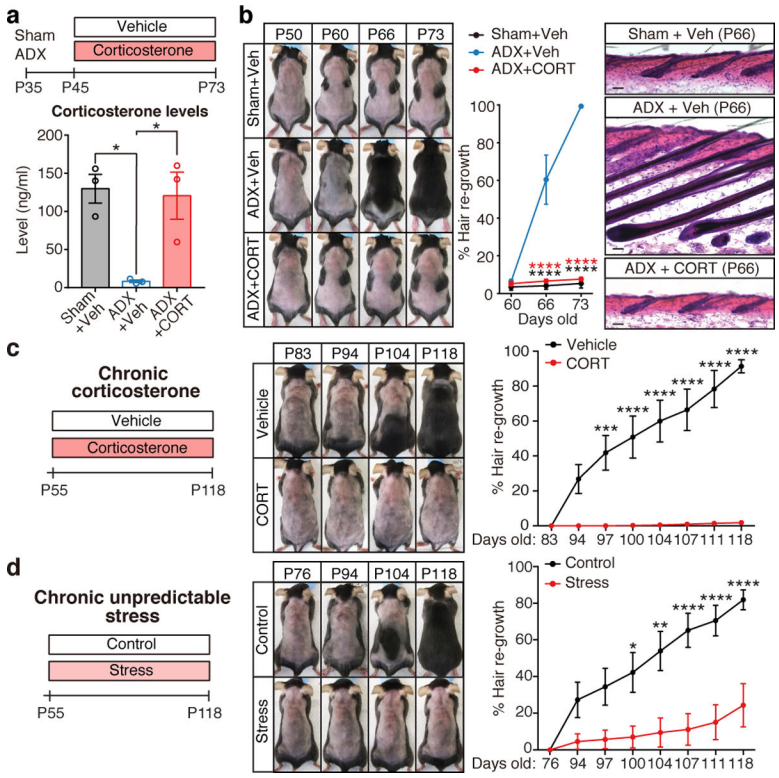

Fig. 2 |. Adrenal gland-derived corticosterone regulates HFSC quiescence.

a, Plasma corticosterone levels in different mice 2 weeks after feeding corticosterone (CORT) or vehicle (Veh). **b**, Hair cycle progression and H&E staining of sham+Veh, ADX+Veh, and ADX+CORT mice. Scale bar, 50 μm. **c**, Hair cycle progression of C57BL/6 mice fed with vehicle or corticosterone. **d**, Hair cycle progression in C57BL/6 mice subjected to chronic unpredictable stress and non-stressed control. Data are mean±s.e.m. $*P < 0.05$, $**P < 0.01$, $***P < 0.001$, $****P < 0.0001$. Exact P values see source data files. Statistics, sample sizes, and numbers of replications are in Methods, 'Statistics and Reproducibility'.

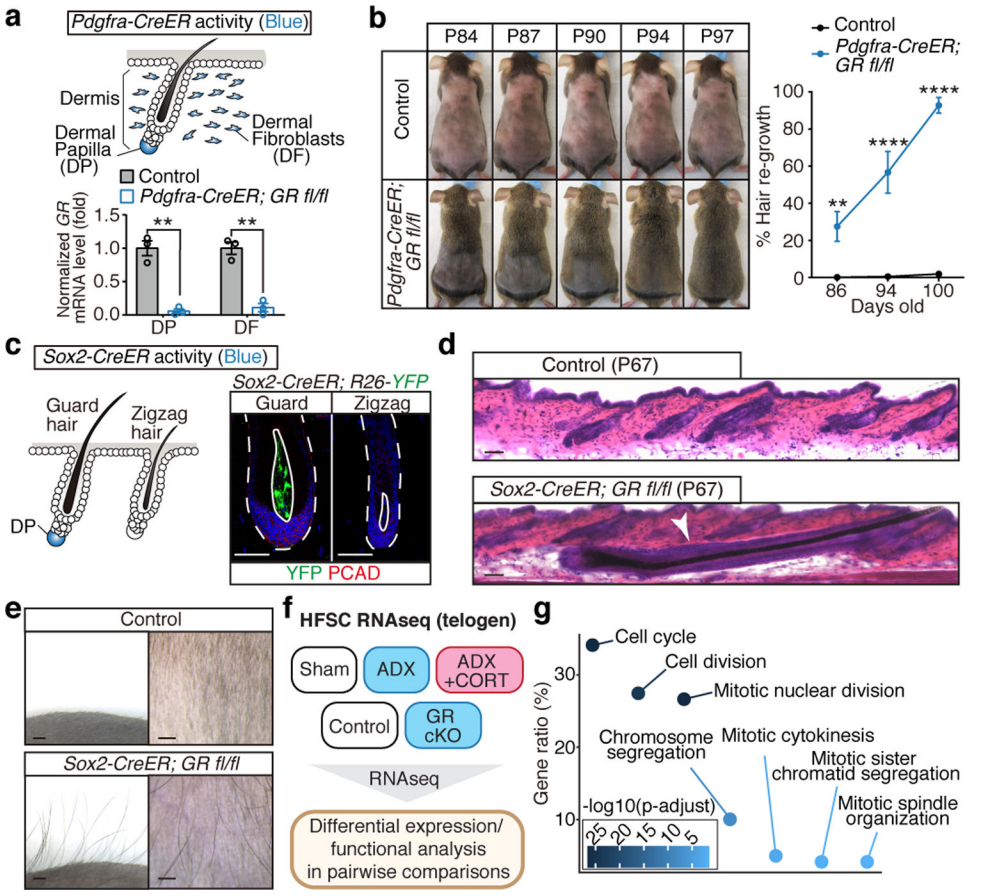

Fig. 3 |. Corticosterone acts on dermal papilla (DP) to regulate HFSC quiescence.

a, *Pdgfra-CreER* depletes *GR* efficiently in DP and dermal fibroblasts (DF). **b**, Hair cycle progression of control and *Pdgfra-CreER;GRfl/fl* mice. **c**, Immunohistochemical analyses (YFP and PCAD) of *Sox2-CreER;R26-lsl-YFP* skin showing YFP in DP of guard HFs but not zigzag HFs. **d**, H&E staining of control and *Sox2-CreER;GRfl/fl* skin (arrowhead: an anagen guard HF surrounded by telogen HFs). **e**, Surface view (side and top) showing accelerated anagen only in the guard hairs in *Sox2-CreER;GRfl/fl* mice (shaved at P45; imaged at P67). **f**, RNAseq workflow. **g**, GO enrichment analysis of 121 shared differentially expressed genes in HFSCs comparing sham vs. ADX, ADX vs. ADX+CORT, and control vs. *Pdgfra-CreER;GRfl/fl* (see also Extended Data Fig. 6). Scale bars, 50 μm (**c**,**d**), 1 mm (**e**). Data are mean±s.e.m. $^{**}P < 0.01$, $^{****}P < 0.0001$. Exact *P* values see source data files. Statistics, sample sizes, and numbers of replications are in Methods, ‘Statistics and Reproducibility’.

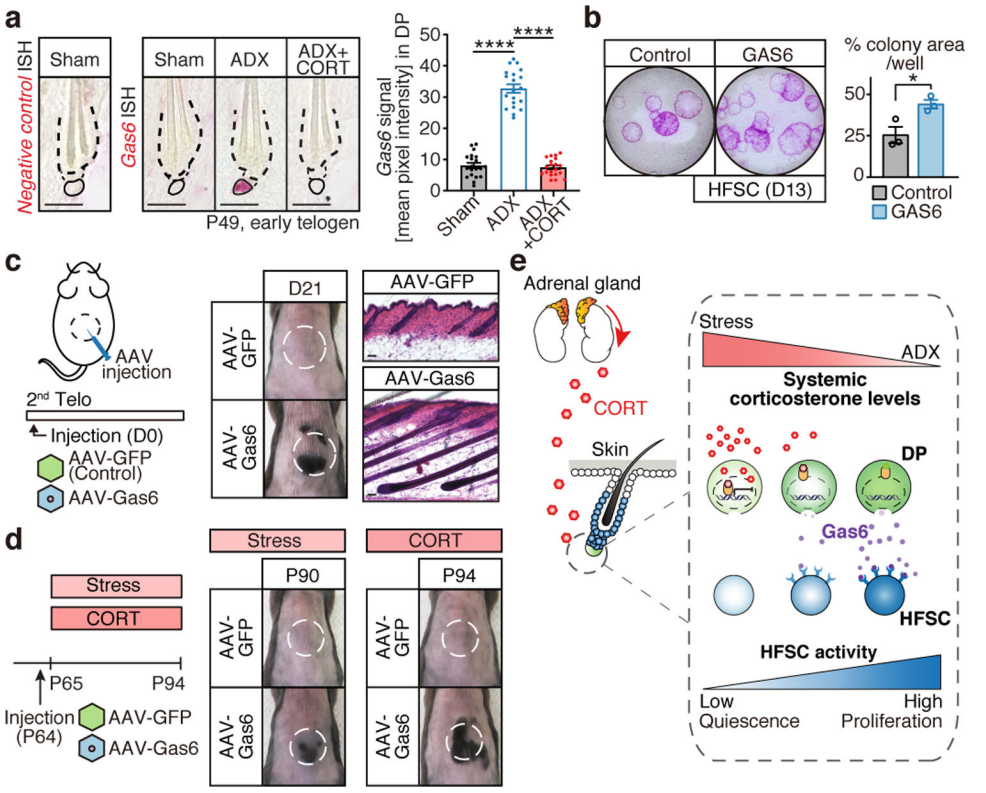

Fig. 4 |. *Gas6* overexpression counteracts the inhibitory effect of corticosterone.

a, Negative control and *Gas6* expression visualized by *in situ* hybridization in early telogen of sham, ADX, and ADX+CORT. Quantification shows *Gas6* signals in DP. Bold dashed lines, bulge; thin dashed lines, hair germ; solid lines, DP. **b**, Cultured HFSCs in the presence or absence of GAS6. **c**, Intradermal injection of AAV-Gas6 but not AAV-GFP induces anagen in injection sites. Dashed circles: AAV injection areas. **d**, AAV-mediated expression of GFP or *Gas6* in mice subjected to chronic unpredictable stress or corticosterone feeding. **e**, Model summarizing main findings. When corticosterone levels drop, elevated *Gas6* expression promotes HFSC activation and anagen entry. Conversely, when corticosterone levels are elevated, *Gas6* expression is inhibited, HFSCs stay in prolonged quiescence. Scale bar, 50 μm (**a**,**c**). Data are mean±s.e.m. *$P < 0.05$, ****$P < 0.0001$. Exact P values see source data files. Statistics, sample sizes, and numbers of replications are in Methods, 'Statistics and Reproducibility'.